Received: 20 March 2019 | Revised: 10 June 2019 | Accepted: 11 June 2019

DOI: 10.1002/dvdy.72

RESEARCH ARTICLE

Developmental Dynamics WILEY

Embryonic development of a parthenogenetic vertebrate, the mourning gecko (*Lepidodactylus lugubris*)

Aaron H. Griffing[1] | Thomas J. Sanger[2] | Juan D. Daza[3] | Stuart V. Nielsen[4] | Brendan J. Pinto[1] | Edward L. Stanley[4] | Tony Gamble[1,5,6]

[1]Department of Biological Sciences, Marquette University, Milwaukee, Wisconsin

[2]Department of Biology, Loyola University in Chicago, Chicago, Illinois

[3]Department of Biological Sciences, Sam Houston State University, Huntsville, Texas

[4]Department of Herpetology, Florida Museum of Natural History, Gainesville, Florida

[5]Milwaukee Public Museum, Milwaukee, Wisconsin

[6]Bell Museum of Natural History, University of Minnesota, Saint Paul, Minnesota

Correspondence
Aaron H. Griffing, Department of Biological Sciences, Marquette University
P.O. Box 1881, Milwaukee, WI 53201.
Email: aaron.griffing@marquette.edu

Funding information
Division of Environmental Biology, Grant/Award Numbers: 1657662, 1657656; Division of Biological Infrastructure, Grant/Award Number: 1701714

Abstract

Background: One goal of evolutionary developmental biology is to understand the role of development in the origin of phenotypic novelty and convergent evolution. Geckos are an ideal system to study this topic, as they are species-rich and exhibit a suite of diverse morphologies—many of which have independently evolved multiple times within geckos.

Results: We characterized and discretized the embryonic development of *Lepidodactylus lugubris*—an all-female, parthenogenetic gecko species. We also used soft-tissue μCT to characterize the development of the brain and central nervous system, which is difficult to visualize using traditional microscopy techniques. Additionally, we sequenced and assembled a de novo transcriptome for a late-stage embryo as a resource for generating future developmental tools. Herein, we describe the derived and conserved patterns of *L. lugubris* development in the context of squamate evolution and development.

Conclusions: This embryonic staging series, μCT data, and transcriptome together serve as critical enabling resources to study morphological evolution and development, the evolution and development of parthenogenesis, and other questions concerning vertebrate evolution and development in an emerging gecko model.

KEYWORDS

brain, embryology, Gekkota, reptile, staging table, transcriptome, μCT

1 | INTRODUCTION

A central goal of evolutionary-developmental (evo-devo) biology is to understand the developmental changes that result in phenotypic novelty and convergence. Interest in how developmental processes have influenced morphological diversity has led to the recent investigation of squamate (lizard, snake, and amphisbaenian) development. These studies have demonstrated the immense utility of squamates as models for the development of amniote *bauplans*.[1-7] Ideally, model clades or species in evo-devo will meet several criteria (reviewed by Jenner and Wills[8]). First, the primitive character states and subsequent evolution of derived character states should be known in a phylogenetic framework. Second, the study of this clade, or species, should reveal some combination of unique, derived patterns and broad, conserved patterns. Finally, the clade or species should be practical to rear in a laboratory setting and have available resources to facilitate the investigation of evo-devo questions.

Gecko lizards (Gekkota) are a clade that exemplifies these criteria. The gecko *bauplan* is considered similar to the ancestral squamate form[9] while also exhibiting several derived morphologies, such as adhesive toepads, which have independently evolved numerous times within gecko evolutionary history.[10-13]

Homoplasies (convergent character states), such as this, have been uncovered with robust phylogenetic analyses of gecko relationships.[10,14,15] Recent phylogenetic studies using molecular data find high support for geckos, with the exception of dibamid lizards, as the sister clade to remaining squamates.[16,17] Therefore, geckos are an integral component for studies exploring the full range of comparative squamate evo-devo. This combination of the ancestral *bauplan*, complex, derived morphologies, rampant convergence on numerous character states, and robust phylogenetic hypotheses make geckos the ideal group to study gecko-specific derived patterns, as well as enlighten squamate- or vertebrate-wide conserved patterns. Logistically, many gecko species have simple protocols for their husbandry, can be reared in space-efficient enclosures, and have an increasing number of genomic resources that are available or in development.[18-24]

Of more than 1800 described species of gecko,[25] the Mourning Gecko (*Lepidodactylus lugubris*) stands out as an ideal model to study developmental questions. *Lepidodactylus lugubris* is a small-bodied gecko native to Southeast Asia and nearly all Pacific islands.[18,26,27] This species belongs to the pan-Asian *Gekko* clade of gekkonid lizards, including the charismatic gliding geckos (*Ptychozoon*), flap-legged geckos (*Luperosaurus*), true geckos (*Gekko*), and slender geckos (*Pseudogekko*[15,28,29]). Like many other species in this clade, *L. lugubris* exhibits distally divided basal toe pads, which facilitate digital adhesion.[13] Gekkonid lizards, such as *L. lugubris*, are oviparous; they reproduce by laying hard-shelled eggs, and have a fixed clutch-size of two eggs.[30] Arguably, the most interesting aspect of *L. lugubris* biology is parthenogenesis. This species is composed almost entirely of females, which reproduce successfully without male gametes, resulting in clonal daughters that are genetically identical to mothers (i.e., obligate parthenogenesis[31]). Male phenotypes are occasionally encountered in the wild or in captivity, however these individuals are extremely rare and typically infertile.[31-33] Numerous clonal lineages have been described for *L. lugubris*, each of which are considered to have been derived from separate hybridization events between *Lepidodactylus moestus* and an as of yet undescribed *Lepidodactylus* species from the South Pacific.[34] Interestingly, backcrosses between diploid ($2n = 44$) *L. lugubris* lineages and one of the parental species can result in triploid ($3n = 66$) clonal lineages.[34,35] Thus, *L. lugubris* is a suitable model to study morphological development, phenotypic plasticity, sexual development, and the evolution of changes in ploidy.

Parthenogenetic organisms are ideal study systems for developmental studies for several reasons: (a) every individual in a laboratory colony, after reaching sexual maturity, is reproductively active (i.e., no "2-fold" cost of sex[36]), (b) there is no need for mate pairing, and (c) individuals within a clonal lineage should theoretically be genetically identical. Despite these factors, few parthenogenetic vertebrates are routinely maintained in laboratory settings.[37-42] Several additional characteristics make *L. lugubris* a desirable model organism, including reproductive output (they are highly fecund, laying eggs year round[43]), there are published protocols for husbandry and embryo collection,[18] they can easily be targeted for field collection (including from populations in the Hawaiian Islands[26]) or commercial purchase, and, unlike the majority of squamates, have hard-shelled eggs which make embryological dissection and manipulation substantially easier.[5]

Embryonic staging series, or normal staging tables, are valuable foundational tools for the study of new and diverse developmental model systems.[44-48] Detailed descriptions of embryonic development facilitate effective experimental design and allow for an understanding of the timing of major developmental events. Since the first squamate embryonic staging series was generated almost 115 years ago (*Lacerta agilis*[49]), another 34 complete squamate embryonic staging series have been published (Lima et al[50]; reviewed in References 51-53), thus providing ample comparative material for broad investigations into trends of squamate evolution and development.

Staging tables are not the only resource needed by modern developmental biologists. Genomic and transcriptomic resources are necessary for studying spatial and temporal aspects of gene expression during development. Having sequence information for gene families, such as bone morphogenetic proteins (BMPs), which are critical for myriad functions during embryogenesis (e.g., mesoderm formation and patterning, neural patterning, skeletal development, and so forth; reviewed in Reference 54), will allow for the designing and generation of qPCR primers and in situ hybridization probes. Other tools, such as micro-computed tomography (μCT), have facilitated new view of staging series that can, for example, accurately trace ossification sequence of skeletal elements.[52,53,55,56] Despite what seems to be a renaissance of embryological work, few embryonic staging series of reptiles have utilized soft-tissue μCT imaging.[57] Using soft-tissue μCT techniques for embryological characterization provides the opportunity to nondestructively track ossification sequence, as well as, detail the subtleties of visceral, limb, craniofacial, or neural development.[58,59]

Combining light microscopy with soft-tissue μCT imaging, we herein describe the embryonic development of an emerging evo-devo model species, *L. lugubris*, and provide an annotated de novo transcriptome of a late-stage *L. lugubris* embryo as a resource for future evolutionary and developmental investigations. Data generated by this study, particularly the open-access transcriptomic and μCT data, taken together, provide ample resources for the continued study of *L. lugubris* as an evo-devo model and sets the foundation for the expansion of integrative developmental studies in squamates.

2 | RESULTS

2.1 | Characterization of external morphology

We diagnosed 16 developmental stages using a numbering scheme commonly used for squamates.[60-62] Stage 28 corresponds to stage at oviposition and stage 43 corresponds to a stage that directly precedes hatching. Although temperature can significantly affect the length of incubation,[63] our sample of 242 embryos ranged from 0 days post-oviposition (dpo) to 77 dpo (Figure 1).

Stage 28 (Figure 2A,B)

Mean SVL: 4.11 mm (Standard deviation [sd] = 0.18, n = 3).

Neural: There is little cephalic bulging (Figure 2A). The mesencephalon is distinct from the metencephalon and diencephalon, and the telencephalon is distinct from the diencephalon (Figure 2B). The margin of the otic capsule is faintly visible and translucent. The neural tube is open along the dorsum, starting anteriorly at the metencephalon and open most posteriorly at the first three somites.

Pharyngeal arches and facial prominences: Pharyngeal clefts 1–2 are distinct (Figure 2B). Pharyngeal arches I–III are distinct (Figure 2B). Facial primordia are present but unfused.

Eye: The eye is completely unpigmented (Figure 2B). The optic cup is circular in shape and the margin of the lens is round but irregular in shape. The choroid fissure margins are in contact and in the process of fusing.

Limbs: Limb buds are only present as small, barely visible swellings.

Thorax and tail: 30–32 somites. The endocardial tube is prominent and beating. Liver formation is indicated by condensed tissue directly posterior to the endocardial tube (Figure 2B). The nephrogenous mesenchyme, which currently lacks mesonephric tubules and gives rise to the mesonephros, is visible.

Flexures and rotation: The cranial flexure is underway with the axes of the hind- and forebrains at an acute angle. The dorsal contour from the mesencephalon to the tail is curved, with the lumbo-sacral region exhibiting a more extreme curve (Figure 2A).

Stage 29 (Figure 2C–E)

Mean SVL: 6.30 mm (sd = 0.42, n = 5).

Neural: A dorsal mesencephalic bulge (i.e., the developing optic tectum) is prominent (Figure 2C). The myelencephalic, metencephalic, and diencephalic bulges are present but less distinct than mesencephalon (Figure 2D). The diencephalic-telencephalic boundary is visible. The otic capsule is still translucent but the margin is much more distinct than the previous stage.

Eye: The retinal pigmented epithelium (RPE) is beginning to pigment. The optic cup is more ovoid in shape, expanding posteriorly. The lens is less irregular in shape than the previous stage. The choroid fissure is closing, but not yet fully fused (Figure 2D).

Pharyngeal arches and facial prominences: Pharyngeal clefts 1–3 are present and distinct. Pharyngeal arch I is separated into the maxillary arch and the mandibular arch. Pharyngeal arch II now obscures the majority pharyngeal arch III and pharyngeal cleft 2. Pharyngeal arch IV is visible. The

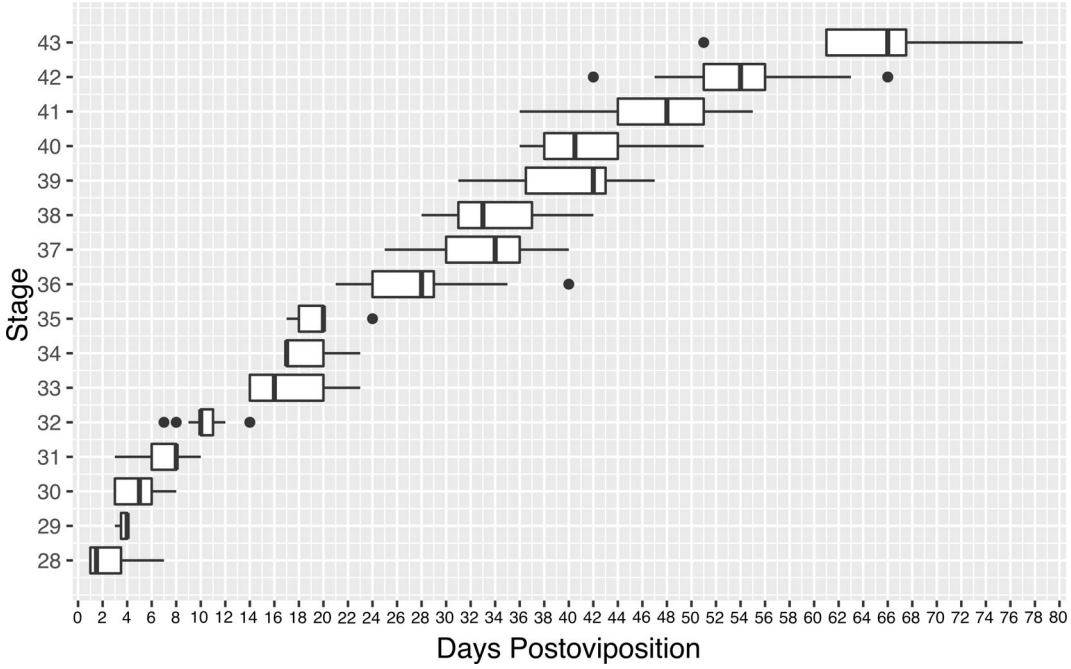

FIGURE 1 The observed ranges of post-ovipositional stages defined in this study when incubated at 26°C. Black circles correspond to outliers

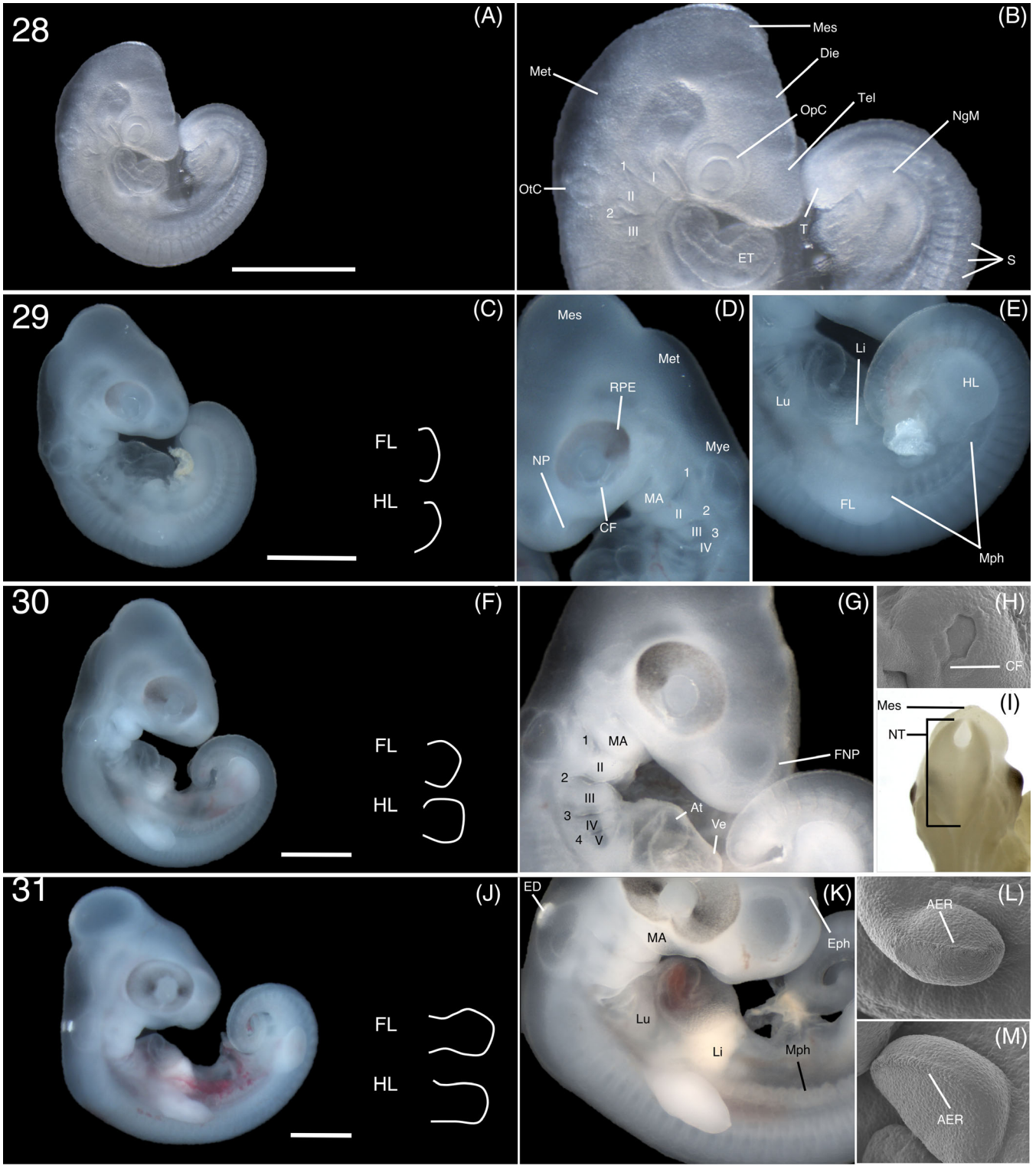

FIGURE 2 Stages 28–31 of *Lepidodactylus lugubris* embryonic development. Stage 28: lateral view of the whole embryo (A) with closer view of the cranial region (B). Stage 29: lateral view of the whole embryo and illustration of the limbs (C), closer view of the cranial and pharyngeal regions (D), and closer view of the thorax (E). Stage 30: lateral view of the whole embryo and illustration of the limbs (F), closer view of the cranial and pharyngeal regions (G), SEM image of the eye (H), and dorsal view of the neural tube of a preserved embryo (I). Stage 31: lateral view of the whole embryo and illustration of the limbs (J.), closer view of the pharyngeal and thoracic regions (K), and closer views of a SEM forelimb (L) and hindlimb (M). Scale bars = 1 mm. 1–4, pharyngeal clefts 1–4; I–V, pharyngeal arches I–V; AER, apical ectodermal ridge; At, atrium; CF, choroid fissure; Die, diencephalon; ED, endolymphatic duct; Eph, epiphysis; ET, endocardial tube; FNP, frontonasal prominences; FL, forelimb; HL, hindlimb; Li, liver; Lu, lungs; MA, mandibular arch; Mes, mesencephalon; Met, metencephalon; Mph, mesonephros; Mye, myelencephalon; NgM, nephrogeneous mesenchyme; NP, nasal pits; OpC, optic cup; Otc, otic capsule; RPE, retinal pigmented epithelium; S, somites; T, tail; Tel, telencephalon; Ve, ventricle

maxillary arch fused anteriorly to the cranial region. The nasal pits are present (Figure 2D). Facial primordia have yet to fuse.

Limbs: Both hindlimb and forelimb buds are present and are similar sizes (Figure 2C,E).

Thorax and tail: 40–41 somites extending into the tail. The liver is now opaque and completely visible posterior to the endocardial tube. The lungs are now visible as opaque tissue condensations dorsally adjacent to the endocardial tube. The mesonephros and its tubules are visible directly posterior to the forelimb buds (Figure 2E).

Flexures and rotation: The axes of the hind- and forebrains are at a nearly right angle. The dorsal contour from the mesencephalon to the tail is similar to the previous stage (Figure 2C).

Stage 30 (Figure 2F–I)

Mean SVL: 7.76 mm (sd = 0.81, n = 17).

Neural: The dorsal bulge of the optic tectum is more exaggerated than the previous stage (Figure 2F). The telencephalic bulges are paired and beginning to fuse in the frontal region. The margins of the otic capsule are distinct with the fluid filled inside remaining translucent (Figure 2F, G). The opening of the neural tube is closing from posterior to anterior (Figure 2I).

Eye: The optic cup remains an ovoid shape (Figure 2G). Pigment has now spread to the anterior portion of the eye, though still heaviest at the posterior. The choroid fissure remains only as a faint groove (Figures 2H and 3A).

Pharyngeal arches and facial prominences: The frontonasal prominences are paired and visible. Pharyngeal arch V and pharyngeal cleft 4 is now present (Figure 2G).

Limbs: Both hindlimbs and forelimbs are paddle shaped and similar sizes (Figures 2F and 3B).

Thorax and tail: 45–47 somites. The heart now has a distinct unified atrium and ventricle. The liver is completely opaque white (Figure 2F).

Flexures and rotation: The axes of the cervical and thoracic regions are nearly at a right angle. The contour of the thoracic region to the tail is similar to the previous stage (Figure 2F).

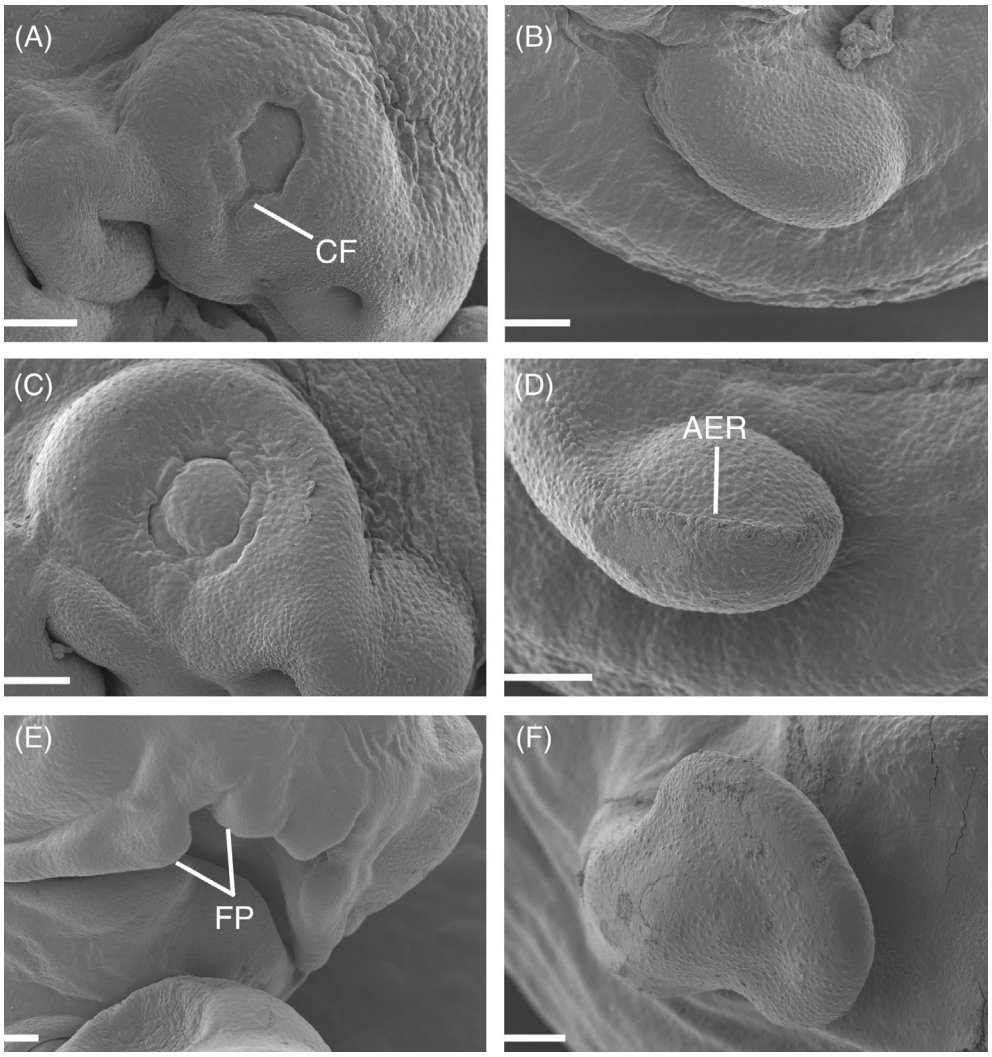

FIGURE 3 Scanning electron micrographs of *Lepidodactylus lugubris* embryos at stages 30 (A, B), 31 (C, D), and 32 (E, F). Lateral views of the eye (A, C), fusing facial primordia (E), and limb development (B, D, F). Scale bars = 100 μm. CF, Choroid fissure; AER, apical ectodermal ridge; FP, facial primordia

Stage 31 (Figure 2J–M)

Mean SVL: 9.69 mm (sd = 0.71, n = 23).

Neural: The dorsal bulge of the optic tectum is more exaggerated than the previous stage (Figure 2J). The endolymphatic ducts are now opaque and separated (Figure 2J,K). The opening of the neural tube is now restricted to its most anterior portion. The otic capsule is more opaque than the previous stage (Figure 2K). The epiphysis (pineal gland) is prominent and located between the frontonasal prominences (Figure 2K).

Eye: The choroid fissure is fused (Figure 3C). The optic cup remains ovoid in shape but has extended slightly along the antero-posterior axis (Figure 2J). The eye is more pigmented, particularly at the equator near the lens and in the dorsal margin of the eye.

Pharyngeal arches and facial prominences: There is fusion of the anterior three pharyngeal arches and clefts (Figure 2K). The mandibular arch spans halfway along the ventral length of the cranium (Figure 2K).

Limbs: The autopodia of the forelimbs, but not the hindlimbs, are paddle shaped with obvious constriction distinguishing them from the zeugopodium from the rest of the limb (Figure 2J). The apical ectodermal ridge (AER) is present in both fore- and hindlimbs (Figures 2L,M and 3D).

Thorax and tail: The somites are now present along the majority of the tail (Figure 2J). The tail is looping and exhibits a blunt distal tip. The cloaca is clearly visible proximal to the tail and exhibits subtle swellings of adjacent tissue. The heart is less bulbous and exhibits two atria. The liver has grown in size from the previous stage (Figure 2K). The lungs and mesonephros are more opaque than previous stages (Figure 2K). The mesonephros visibly spans from the posterior portion of the liver to the hindlimb.

Stage 32 (Figure 4A–D)

Mean SVL: 10.12 mm (sd = 0.72, n = 18).

Neural: The optic tectum has grown (Figure 4A,D). The endolymphatic ducts are positioned more medially than the previous stage.

Eye: There is more diffuse pigment, spread equally across the majority of the eye (Figure 4B). Iris development is underway superficial to the RPE and appears as condensed pigment along the margin of the lens.

Pharyngeal arches and facial prominences: The mandibular prominences nearly meet the medial nasal processes (Figures 2E and 4B). The region of the craniofacial prominences does not project far past the anterior margin of the eye.

Limbs: The podial elements (autopodia, zeugopodia, and stylopodia) are distinct in the forelimbs (Figures 2F and 4A). The autopodia are asymmetrical. The autopodia of the hindlimbs are distinct but stylopodium and zeugopodium are not. The AER is a solid, irregular line. The digits have not condensed yet but the blood vessels mark the position where digits will form.

Thorax and tail: The tail has narrowed to a sharp tip (Figure 4A). The heart is less bulbous than the previous stage (Figure 4C). The liver now exhibits distinct lobes, is more pigmented, and is more vascularized (Figure 4A). The gallbladder is visible as a small green-brown spot on the ventral side of the liver (Figure 4C). The mesonephros is more pigmented and vascularized than the previous stage. Paired cloacal swellings are visible, indicating the onset of cloacal and hemiphallic development.

Stage 33 (Figure 4E–G)

Mean SVL: 11.45 mm (sd = 0.57, n = 11).

Neural: The optic tectum is now its largest relative to the cranial region of the embryo (Figure 4E). The endolymphatic ducts are nearly touching medially.

Eye: The eye exhibits much denser pigment. The pupil is now readily defined based on pigmentation of the iris (Figure 4E).

Pharyngeal arches and facial prominences: All pharyngeal clefts are fused. The maxillary prominence has fused with the medial-nasal. The facial region has elongated anterior to the eye. The mandibular prominence does not extend to the tip of the face (Figure 4F).

Limbs: Digital condensations are visible and the irregular margins of the autopodia mark where the distal tips of the digits will form and that the reduction of interdigital webbing has begun (Figure 4E,F). The AER is more distinct on digit tips rather than between digits (Figure 4F). All podial elements are distinct in the hindlimbs. The autopodia of both hind- and forelimbs are asymmetrical (Figure 4E).

Thorax and tail: The majority of the viscera, with the exception of the posterior portion of the liver and gallbladder, is enclosed within the body wall and less visible (Figure 4F). The gallbladder exhibits darker color than the previous stage, indicating accumulation of bile. The tail is less coiled than the previous stages. Cloacal swellings and hemiphallus are prominent and easily distinguished using light microscopy (Figure 4G).

Stage 34 (Figure 4H–J)

Mean SVL: 12.46 mm (sd = 0.69, n = 8).

Neural: There are no obvious changes in neural morphology (Figure 4H).

Eye: The eye is heavily pigmented. The outer margin of the iris exhibits a band of lighter coloration and is expanded from the previous stage (Figure 4H,I).

Craniofacial: The embryo has distinct snout which comes in contact with the mandible (Figure 4I). The prominences are no longer visible.

Limbs: All podial elements are elongated (Figure 4H). Interdigital webbing has recessed to the point where the distal tips of the digits are free (Figure 4J). The digits themselves have expanded laterally.

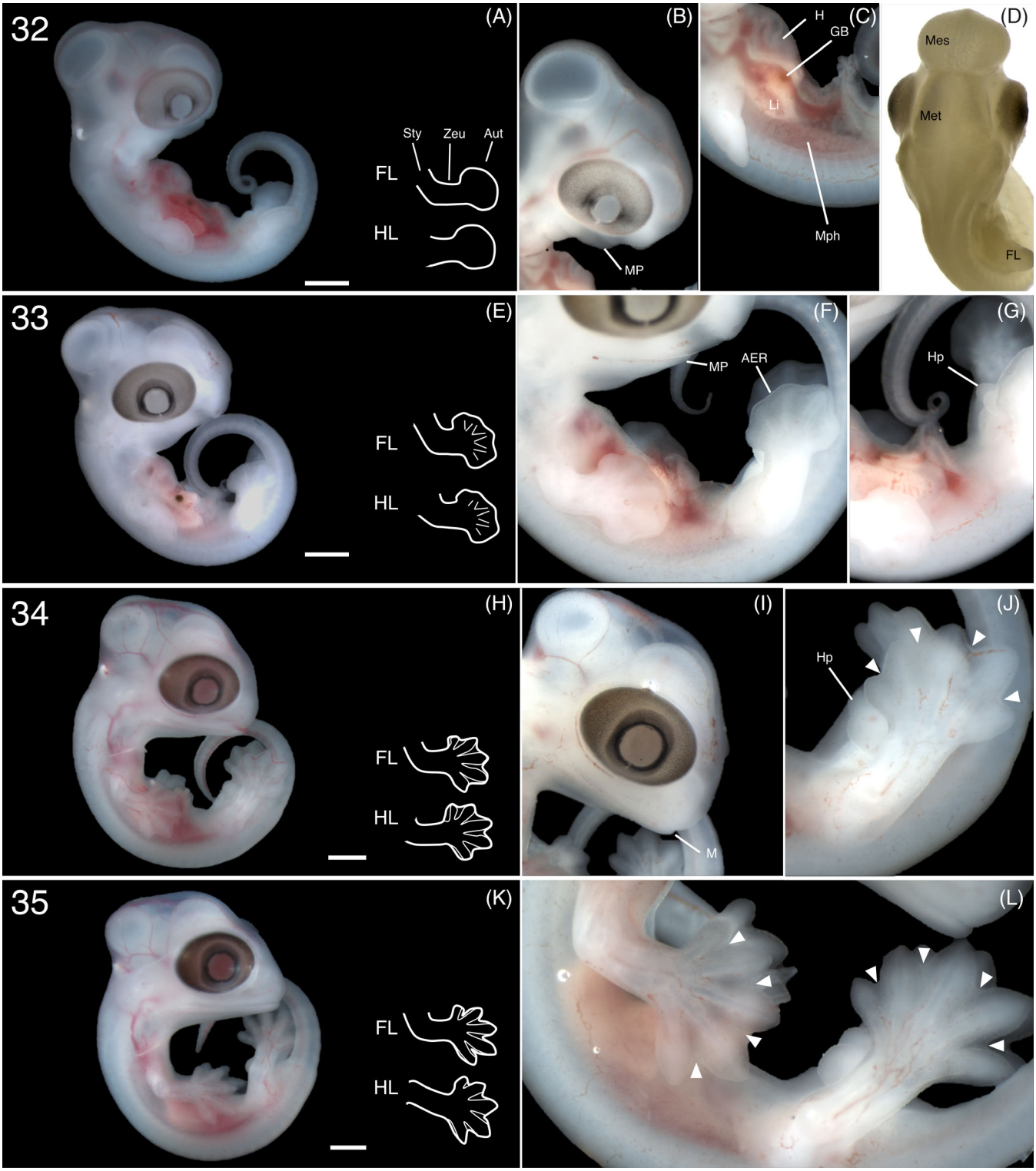

FIGURE 4 Stages 32–35 of *Lepidodactylus lugubris* embryonic development. Stage 32: lateral view of the whole embryo and illustration of the limbs (A), closer view of the craniofacial region (B), closer view of the thorax (C), and dorsal view of the closed neural tube of a formalin-fixed embryo (D). Stage 33: lateral view of the whole embryo and illustration of the limbs (E), closer view of the limbs and the thorax (F), view of the developing cloacal region (G). Stage 34: lateral view of the whole embryo and illustration of the limbs (H), closer view of the craniofacial region (I), and closer view of a hindlimb and the cloacal region (J). Stage 35: lateral view of the whole embryo and illustration of the limbs (K) with closer view of the limbs (L). Scale bars = 1 mm. AER, apical ectodermal ridge; Aut, autopodium; FL, forelimb; GB, gallbladder; H, heart; HL, hindlimb; Hp, hemiphallus; Li, liver; M, mandible; Mes, mesencephalon; MP, mandibular prominence; Mph, mesonephros; Met, metencephalon; Sty, stylopodium; Zeu, zeugopodium. White arrows indicate interdigital webbing recession

Thorax and tail: The body wall is completely closed, covering and obscuring the view of the heart and remaining viscera (Figure 4H). The hemiphallic bulges are more bulbous than the previous stage (Figure 4J). These bulges exhibit morphology more similar to developing hemipenes than hemiclitores in other squamates and will be henceforth be referred to as hemipenes.[64,65]

Stage 35 (Figure 4K,L)

Mean SVL: 12.21 mm (sd = 0.69, n = 2).

Neural: The areas of the brain adjacent to the optic tectum are relatively larger (Figure 4K). The endolymphatic ducts have met medially at the posterior portion of the mesencephalon.

Eye: The overall shape of the eye is still ovoid, with the first signs of the upper and lower eyelid appearing where the eye meets the lateral portion of the face. The overall collection of eye pigment appears darker (Figure 4K). The light band of iris pigment from the previous stage has expanded in size.

Craniofacial: The craniofacial region anterior to the eye (i.e., snout) is further elongated (Figure 4K).

Limbs: All podial elements are further elongated (Figure 4K). Interdigital webbing has recessed further, resulting in a pointed digital condensation (Figure 4L). The digital condensations are wider than the previous stage.

Thorax and tail: The vertebrae are faintly visible through the thorax and the tail (Figure 4K).

Stage 36 (Figure 5A,B)

Mean SVL: 13.98 mm (sd = 1.40, n = 3).

Neural: The other regions of the brain, especially the telencephalon, have increased in size relative to the mesencephalon — the telencephalic bulge and bulge of the optic tectum appear similar in size (Figure 5A).

Eye: The overall shape of the eye remains ovoid on the antero-posterior axis while shape of the iris is circular (Figure 5A). The upper and lower eyelids are visible, overlaying a small portion of iris pigment.

Craniofacial: Craniofacial region more elongate than the previous stage (Figure 5A). The ear is visible and open.

Limbs: Reduction of interdigital webbing is complete (Figure 5B). Skeletal elements of the digits and limbs are visible.

Thorax and tail: The ribs are faintly visible. Each of the two hemipenes is bilobed.

Stage 37 (Figure 5C,D)

Mean SVL: 14.98 mm (sd = 0.84, n = 5).

Neural: The optic tectum is less distinct due to the relative increase in size of the embryo (Figure 5C).

Eye: The eye is superficially similar to the previous stage with the exception that the iris and the pupil have increased in size and the upper and lower eyelids appear fused (Figure 5C).

Craniofacial: The craniofacial region is more elongate (Figure 5C). The ear is distinct and well developed.

Limbs: The digits are more elongate than the previous stage. The distal tip of each digit is and beginning to taper, which will eventually form the claw (Figure 5D). The first subdigital lamellar ridges of the toepads are visible.

Thorax and tail: The ribs are more visible through the body wall than the previous stage. The lobes of each hemipenis are more prominent than the previous stage.

Scales and pigment: Besides the subdigital lamellae, the scales of the hind- and forelimbs are the first visible.

Stage 38 (Figure 5E,H)

Mean SVL: 15.51 mm (sd = 1.13, n = 4).

Neural: The mesencephalon and telencephalon are less distinct (Figure 5E).

Eye: The eye is more rounded and darker in color than the previous stage (Figure 5E). The pupil is rounded and, with the fusion of the eyelids, the brille (i.e., spectacle) is apparent.

Craniofacial: The craniofacial region is more elongate (Figure 5E). The nostrils are faintly visible.

Limbs: Toepad development is well underway with more subdigital lamellae forming and the pads themselves expanding laterally. The claws are now distinct from the rest of the digits and beginning to curve down towards the plantar side of the autopodia (Figure 5F).

Thorax and tail: The hemipenes are completely forked and engorged (Figure 5H).

Scales and pigment: The hind- and forelimb scales are more distinct. The first signs of scales and sparse pigment appear along the dorsal surface of the thorax and head (Figure 5G).

Stage 39 (Figure 5I–L)

Mean SVL: 16.09 mm (sd = 1.39, n = 4).

Neural: The mesencephalon and telencephalon are less distinct (Figure 5I).

Eye: The chromatophores (xanthophores and melanophores) of the iris are visible (Figure 5L). The pupil is ovoid.

Craniofacial: The snout is more elongate (Figure 5I). The first signs of labial scales are present.

Limbs: The toepads continue to expand laterally (Figure 5K). The claw is now fully developed.

Thorax and tail: The ribs are well developed and distinct (Figure 5J). The body wall is more opaque, beginning to obstruct the view of the liver and gallbladder.

Scales and pigment: The dorsal scales are more distinct than the previous stage. The ventral and caudal scales are visible for the first time. Pigment is more widespread along the dorsum (Figure 5J).

Stage 40 (Figure 6A,B)

Mean SVL: 17.60 mm (sd = 1.07, n = 3).

Neural: The mesencephalon and telencephalon are less distinct (Figure 6A).

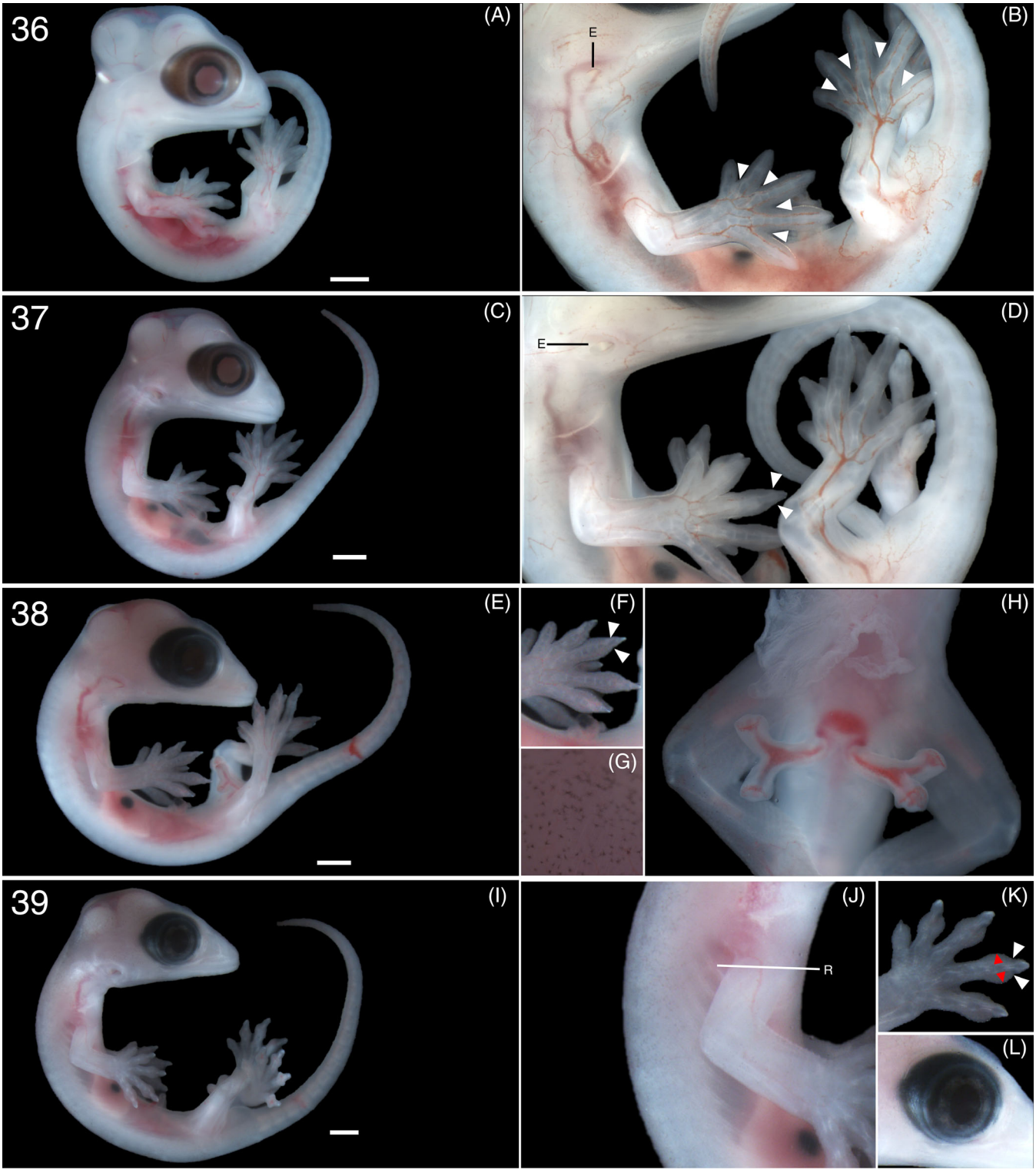

FIGURE 5 Stages 36–39 of *Lepidodactylus lugubris* embryonic development. Stage 36: lateral view of the whole embryo (A) with closer view of the limbs (B). Stage 37: lateral view of the whole embryo (C) with closer view of the limbs (D). Stage 38: lateral view of the whole embryo (E), closer view of the manus (F), closer view of pigmentation density on dorsum (G), and ventral view of the cloacal region exhibiting everted hemiphallus (H). Stage 39: lateral view of the whole embryo (I.), closer view of the thorax (J), closer view of the manus (K), and closer view of the eye (L). Scale bars = 1 mm. E, ear; R, ribs. White arrows indicate tapering of the digit to form the claw. Red arrows indicate lateral expansion of the toepad

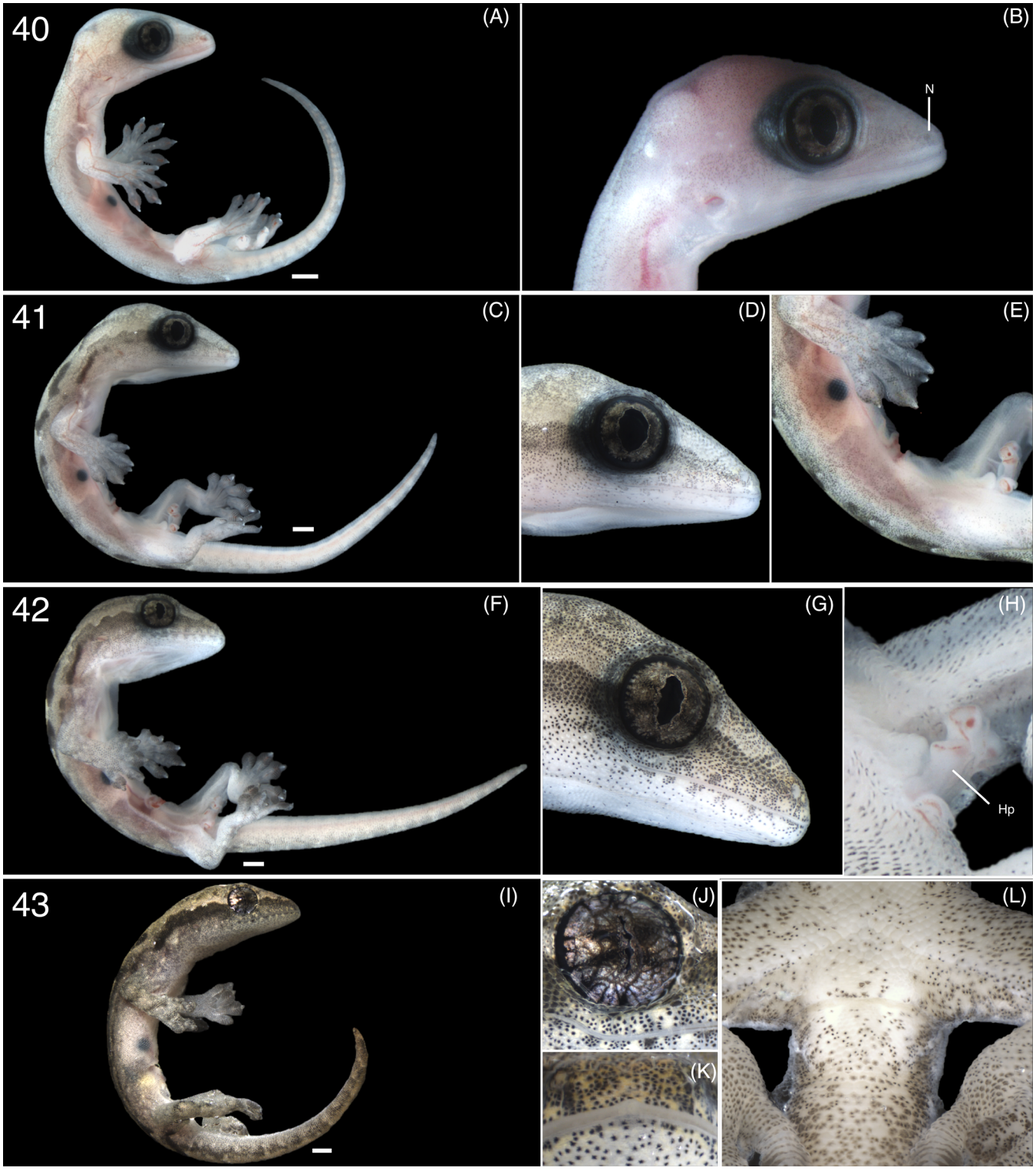

FIGURE 6 Stages 40–43 of *Lepidodactylus lugubris* embryonic development. Stage 40: lateral view of the whole embryo (A) with closer view of the head (B). Stage 41: lateral view of the whole embryo (C), closer view of the head (D), and closer view of the thorax (E). Stage 42: lateral view of the whole embryo (F), closer view of the head (G), and closer view of the cloacal region (H). Stage 43: lateral view of the whole embryo (I), with a closer view of the eye (J), medial view of the mouth (K), and ventral view of the cloacal region exhibiting recessed hemiphallus (L). Scale bars = 1 mm. Hp, hemiphallus; N, external naris

Eye: Yellow coloration, presumably from xanthophores, is denser. The pupil remains ovoid but is thinner than the previous stage (Figure 6B).

Craniofacial: There is no noticeable change in craniofacial region from the previous stage.

Limbs: The toepads continue to expand laterally (Figure 6A).

Thorax and tail: The previous 90° angle of head to the thorax is beginning to open, becoming more obtuse (Figure 6A).

Scales and pigment: The external naris is visible (Figure 6B). The pigment is more widespread across to the body. Pigment is denser in areas, which will eventually become the postnatal coloration patterns (e.g., dorsolateral streak from the snout to posterior of the eye).

Stage 41 (Figure 6C–E)

Mean SVL: 19.24 mm (sd = 4.31, n = 2).

Eye: The pupil is narrower than the previous stage and its vertical slit shape has become irregular.

(Figure 6D).

Limbs: The toepads are now completely developed, taking a bulbous shape approximately half-way up the length of the digit and tapering off again at the claw. The claw is now opaque (Figure 6E).

Thorax and tail: The hemipenes remain everted and forked. Each individual hemipenis lobe is thicker than previous stages (Figure 6E).

Scales and pigment: The labial scales are well defined and the external naris is closed (Figure 6D). Scales and associated pigments have made the dorsal surface of the embryo essentially opaque, thus obscuring the view of the vertebral column, epaxial muscle, and the brain (Figure 6C). The ventral surface remains somewhat translucent, with the liver, gallbladder, and some bones (e.g., ribs, femora) remaining visible (Figure 6C).

Stage 42 (Figure 6F–H)

Mean SVL: 18.31 mm (sd = 1.39, n = 4).

Eye: The pupil is narrower and the irregular shape is forming, that when fully contracted, creates the multiple-pinhole slit pupil (sensu Roth et al.[66]), which is typical of nocturnal gekkotans (Figure 6G).

Thorax and tail: The hemipenes remain everted, yet have stopped growing with the rest of the body, giving the appearance of being smaller (0.75 mm hemipenes, 17.59 mm SVL; stage 42) than the previous stage (0.77 mm hemipenes, 16.50 mm SVL; stage 41) indicating recession into the cloacal region (Figure 6H).

Scales and pigment: The scales are fully developed. The external naris is open. The pigment is denser along the ventrolateral region of the thorax and the ventral surface of the tail (Figure 6F). The ventrum remains somewhat translucent medially (Figure 6F).

Stage 43 (Figure 6I–L)

Mean SVL: 19.54 mm (sd = 1.52, n = 6).

Eye: The pupil fully contracted, creating a multiple-pinhole slit pupil (Figure 6J).

Craniofacial: There are no externally visible egg teeth (Figure 6K; Figure 7).

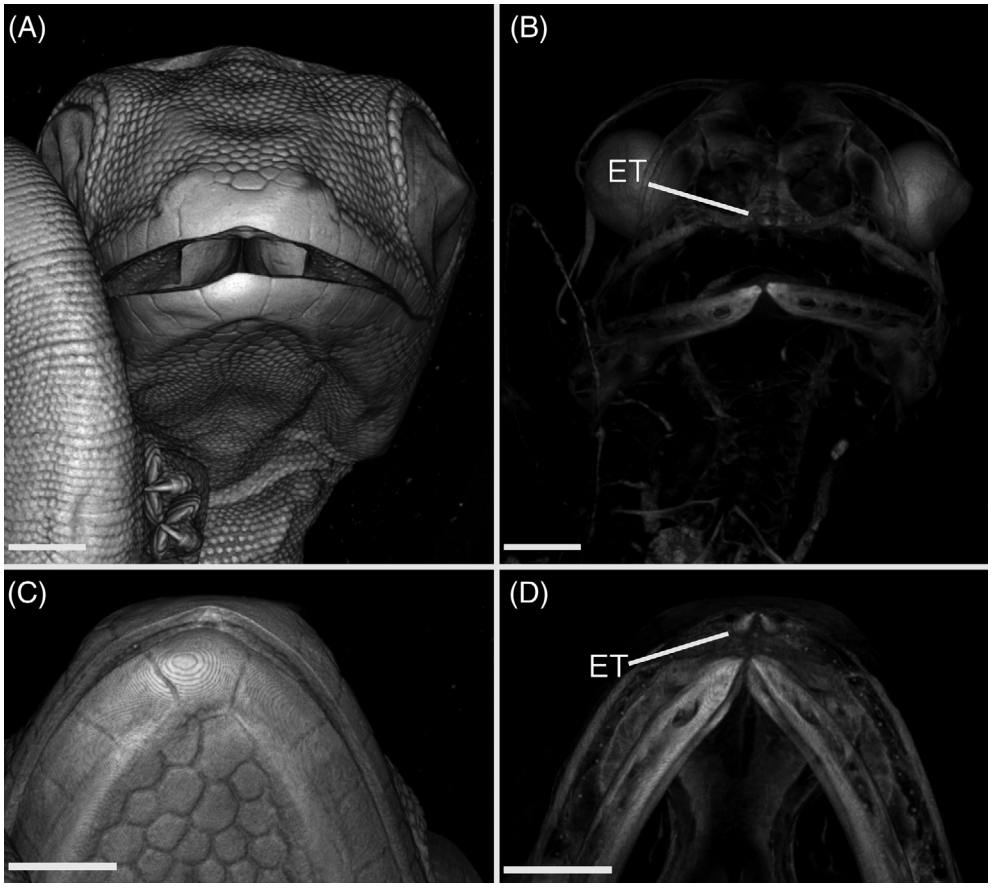

FIGURE 7 Egg teeth (ET) are not externally visible (A, C) but are easily identified using μCT volume rendering (B, D). Mediolateral (A, B) and ventral (C, D) views of a stage 42 *Lepidodactylus lugubris* rostrum. Scale bars = 500 μm

Thorax and tail: The hemipenes are receded (Figure 6L).

Scales and pigment: The scales are opaque, obscuring the view of the viscera, and fully pigmented (Figure 6I).

2.2 | Brain and CNS development

The five secondary vesicles of the embryonic neural tube (i.e., the telencephalon, diencephalon, mesencephalon, metencephalon, and myelencephalon) are often used to define embryonic stages.[6,47,62,67,68] The five vesicles give rise to the following brain structures: the telencephalon gives rise to the cerebral hemispheres and olfactory region; the diencephalon gives rise to the epithalamus, thalamus, and hypothalamus; the mesencephalon gives rise to the optic tectum and tegmentum; the metencephalon gives rise to the tegmentum and the cerebellum; finally, the myelencephalon gives rise to the medulla oblongata.[67-69] Following previous brain developmental series of *Podarcis siculus*,[69] we produced an approximate sequence of gross morphological changes in four of the main regions of the developing *L. lugubris* brain: telencephalon + diencephalon region (TD), optic tectum, cerebellum, and the remainder of the hindbrain. Although the identification of these structures is approximate, we believe the overall descriptions of these main regions might facilitate understanding of large regions of the brain, but we mention some important regions that are easy to visualize in tomography. The μCT-reconstructed series of brain development is illustrated in Figure 8.

At stage 30, the TD shows a clear anterior region that corresponds to the cerebral hemisphere, a ventrally directed region or thalamus, and a superior region or epithalamus. One of the most prominent regions is the optic tectum, which protrudes on the dorsal surface of the head. The optic tectum lies between the telencephalon and the cerebellum. The cerebellum at this state is elongated and runs parallel to the rest of the hindbrain. The hindbrain is nearly straight, having a slight flexure and not wider than the spinal cord. Dorsal to the TD, a small knob projects dorsally representing the pineal gland. At stage 31, the cerebral hemisphere grows proportionally larger, reaching a similar size to the tectum. On the ventral surface of the TD, the pituitary gland is exhibited as a small projection. At stage 32, the optic tectum becomes the most prominent structure of the brain and the cerebellum folds. At stage 33, the olfactory bulbs appear and project anteroventrally. The cerebellum begins expanding towards the hindbrain. The pineal gland is distinct on the dorsal surface of the TD. At stage 34, the olfactory bulbs elongate, the hindbrain becomes slightly larger in diameter than the spinal cord. At stage 35, the olfactory bulbs extend approximately four times the size in the previous stage and the optic nerve extends anteroventrally from the TD. The hindbrain curvature is more marked, to the point that this structure is mostly horizontal, followed by a cervical flexure that indicates the limit with the spinal cord. At stage 36, the cerebral hemisphere expands dorsally. The cerebellum and optic tectum are relatively smaller than the cerebral hemisphere. The cerebellum is embedded on the hindbrain. At stage 37, the size of the optic tectum is sub-equal to the size of the cerebral hemispheres. At stage 38, the anterior portion of the olfactory bulbs starts expanding. Between stages 40 and 43, the expansion of the olfactory bulbs is more evident. The proportions of all the brain parts remain equal, but the brain increases its size.

2.3 | Transcriptome assembly

We generated our final de novo transcriptome assembly from 18,394,074 raw read pairs. This assembly contained 115,656 transcripts with a total length of 129,611,368 bases (bp), with transcripts ranging from 201 bp to 15,792 bp in length. The TransRate assembly score attempts to assess the reliability and completeness of the assembly by calculating the geometric mean of contig scores and multiplying by the ratio of mapped/unmapped raw reads.[70] Our assembly queried a total of 58% of the reference *Gekko japonicus* peptides, which provided 32,823 conditional Reciprocal Best BLAST hits, to generate a modest TransRate assembly score of 0.0926. We assessed the completeness of this transcriptome by comparing its content against databases of conserved orthologs for tetrapods (tetrapoda_odb9; 3,950 genes) and core vertebrate genes (CVG; 233 genes). Against the database of conserved tetrapod genes, our assembly contained a total of 2,029 (51.4%) complete and single-copy orthologs, 1,248 (31.6%) complete and duplicated orthologs, 388 (9.8%) fragmented orthologs, and 285 (7.2%) missing genes; while against the CVG database, our assembly contained 209 (89.70%) complete orthologs, 226 (97.0%) complete and partial orthologs, and was missing only 7 (3.00%) of genes. Indeed, our assembly possesses at least a partial assembly of 92.8% conserved tetrapod orthologs (tetrapoda_odb9) and 97.0% CVG.

There are 10 BMPs annotated in the *G. japonicus* genome, and we were able to confirm nine in our *L. lugubris* transcriptome assembly (BMPs 1–8, and 11). We used a subset of paralogous BMP genes that are hypothesized to be recently diverged[71] to construct a gene tree to validate the accuracy of assigning these paralogs to their respective ortholog (Figure 9). Indeed, we found that each BMP paralog was present, correctly annotated, and the topology of the tree was similar to a Ducy and Karsenty's[71] gene tree at well-supported nodes.

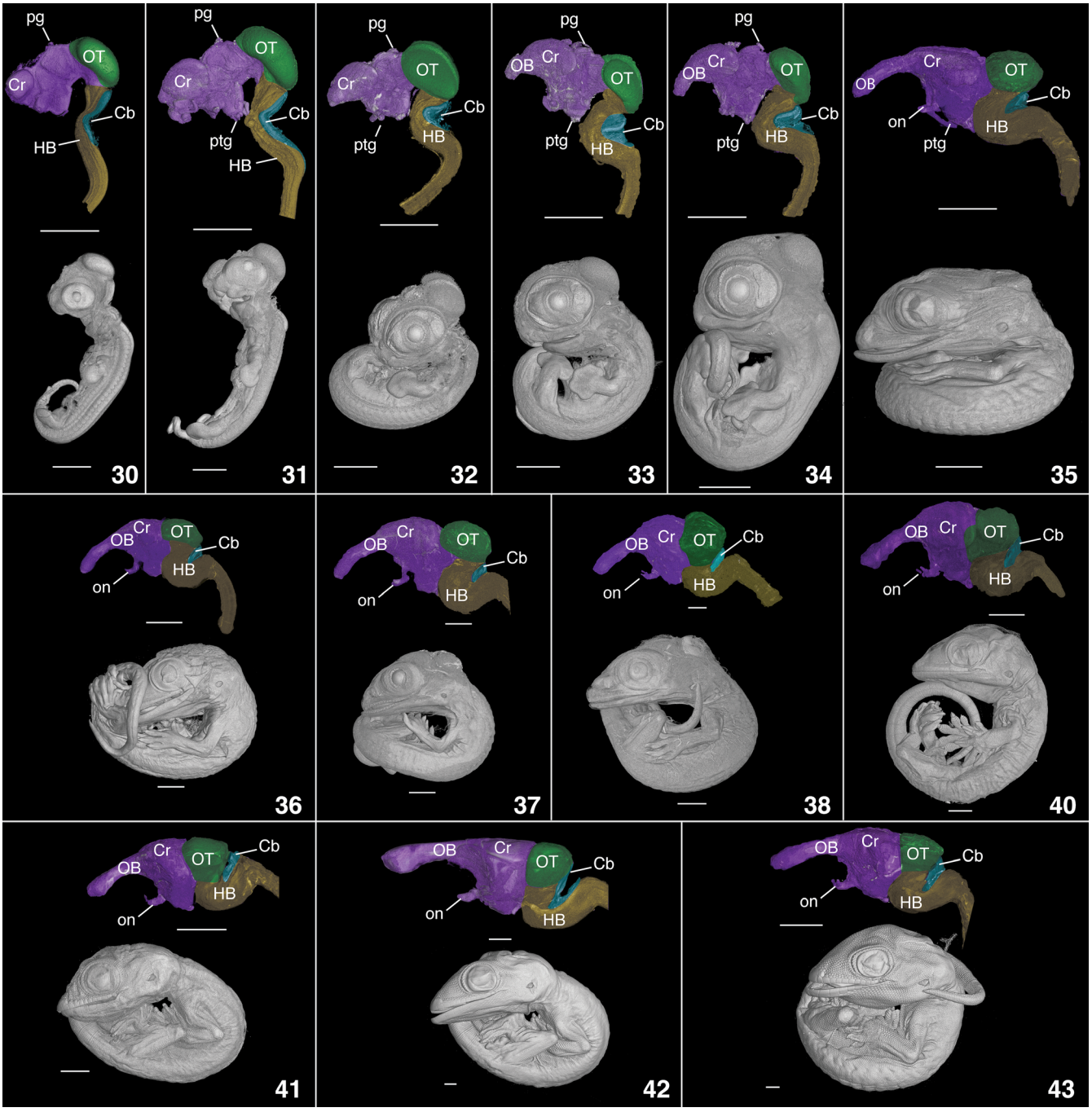

FIGURE 8 Embryonic development of the *Lepidodactylus lugubris* brain visualized through soft-tissue μCT. Whole-embryo μCT images are pictured below the corresponding isolated brain. The four distinct regions of the brain are color-coded as follows: telencephalon + diencephalon, purple; Optic tectum, green; Cerebellum, blue; Hindbrain, yellow. Scale bars = 1 mm. Cb, cerebellum; Cr, cerebrum; HB, hindbrain; OB, olfactory bulbs; ON, optic nerve; OT, optic tectum; pg, pineal gland; ptg, pituitary gland

3 | DISCUSSION

This description of *L. lugubris* embryonic development is the sixth complete staging series of a gecko[6,53,61,62,72] and the first staging series of an obligate parthenogenetic vertebrate. Similar to all other geckos investigated to date, eggs of *L. lugubris* are oviposited during embryo organogenesis.[73] However, the precise developmental stage at oviposition varies between examined gekkotans without apparent phylogenetic specificity. *Tarentola annularis* (Phyllodactylidae) are oviposited at stage 29 and *Paroedura picta* (Gekkonidae) are oviposited approximately at stage 24 (sensu[6,60,61]). The remainder of examined geckos, *L. lugubris* (Gekkonidae), *G. japonicus* (Gekkonidae), *Hemidactylus* sp. (Gekkonidae),

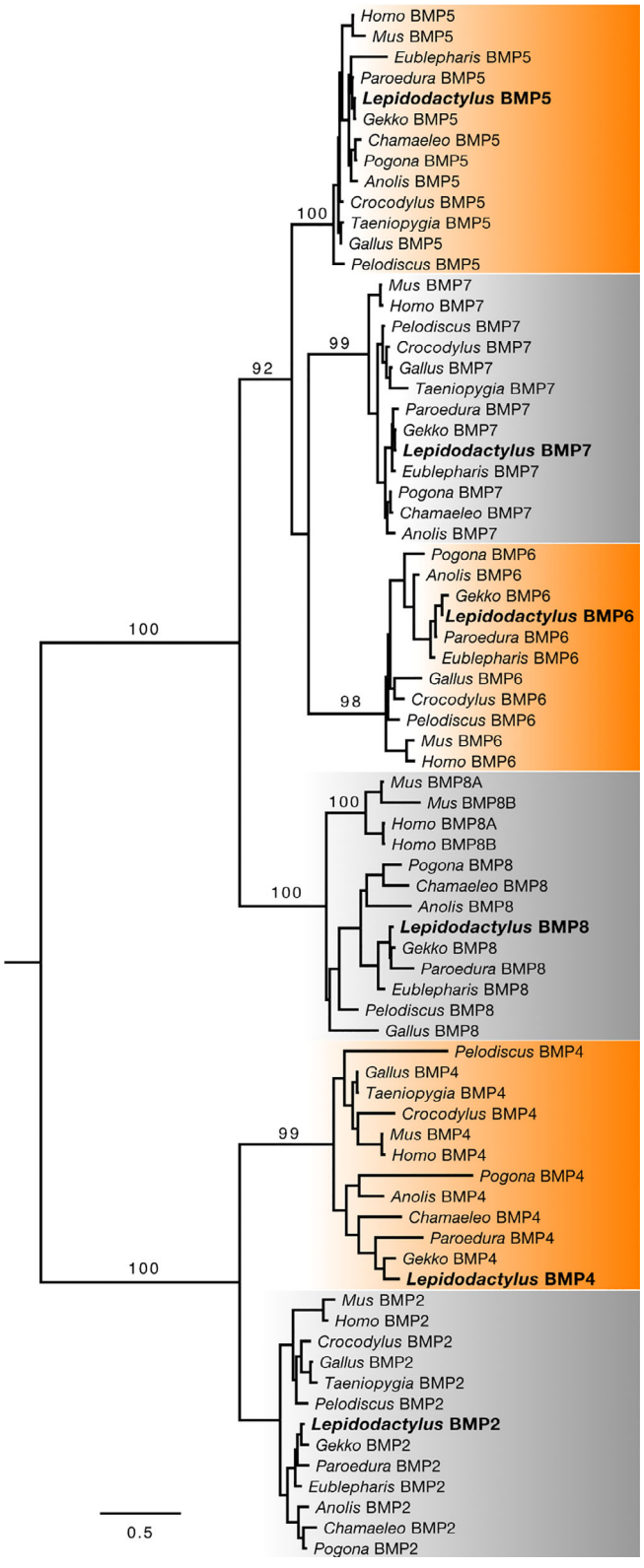

FIGURE 9 Maximum-likelihood gene tree of paralogous BMP sequences. Each paralogous BMP gene clade is highlighted in alternating colors/shades. All short, terminal nodal support values were removed for clarity, while at deeper nodes, only bootstrap support >70 are shown. Tree was rooted at the divergence between BMP2/4 and BMP5-8. Scale bar is in substitutions per-site

and *Eublepharis macularius* (Eublepharidae) oviposit eggs at stage 28.[53,62,72] Indeed, more taxonomic sampling is required to identify any trends in oviposition stage across geckos. However, the average developmental time between oviposition and hatching is longer for *L. lugubris* than most non-gekkotan squamates studied, but similar to other hard-shelled gekkotan eggs (60–65 dpo). For example, the time between oviposition and hatching for *Anolis sagrei* (Pleurodonta) is 22–27 dpo.[47] The longer incubation time of hard-shelled gecko eggs is likely due to lower amounts of gas exchange across the eggshell and thus lower amounts of oxygen available to the embryo.[74,75]

Prior to this study, little was known about *L. lugubris* development. Digital ossification of *L. lugubris* is discussed in-depth by Rieppel.[76] In short, phalangeal ossification occurs in a typical proximo-distal direction; however, *L. lugubris* and *Gehyra oceanica* (Gekkonidae) exhibit delayed ossification in the shortened intermediate phalanges of digits III and IV of both the manus and pes. Delayed ossification of the second phalanx of digit IV is hypothesized to be a consequence of gekkotan digital paedomorphosis, another aspect that departs from the ancestral squamate *bauplan*.[76,77] This developmental delay often results in the loss of this element in some gecko lineages (e.g., *Asaccus*[77]). Gekkonids develop mineralized egg teeth between stages 39 and 40.[78] Although egg teeth are not externally visible in any embryonic stages of *L. lugubris* (Figure 6K), μCT data along with cleared and stained data from Kluge[79] corroborates their presence in the pre-hatchling stages. The egg teeth are paired, erupting from the premaxilla, each directed medially to form a single point (Figure 7), a trait shared by several other gekkonid species.[80]

A striking result of our investigation of *L. lugubris* is the presence and persistence of hemipenis-like structures throughout embryonic development in an all-female species. In the lizard *Anolis carolinensis* and *Anguis fragilis*, paired phalluses develop in both sexes; however, hemipenes are large in males and hemiclitores are small in females.[64,81,82] However, other lizards, such as *Pogona vitticeps* and *Barisia imbricata*, have female embryos with large, hemipenis-like organs that are equal in size and shape with males, that subsequently regress prior to and just after hatching, respectively.[65,83] Our results, coupled with results from the recent literature, make it clear that many aspects of squamate sexual development warrant more detailed examination. Further investigation of external genital development in *L. lugubris* will be discussed in-detail separately.

Gekkotan development has been characterized by the following: later appearance of the paired hemiphallic bulges when compared to other squamates (excluding gymnophthalmids[84]), appearance of the three podial elements later than acrodonts but earlier than pleurodonts,[84] larger relative pupil diameter than pleurodonts and lacertids,[85] and earlier fusion of facial

primordia than pleurodonts.[85] Indeed, pupil diameter of embryonic gekkotans, including *L. lugubris*, is relatively larger than pleurodont and lacertid pupils.[47,86] However, *L. lugubris* exhibit deviations from the other three gecko-specific character states. Paired hemiphallic bulges of *L. lugubris* appear at stage 32, which is later than the gecko *P. picta*, the same timing as some pleurodonts, acrodonts, and gymnophthalmids, but earlier than anguimorphs, and later than other pleurodonts and lacertids.[6,50,60,85,87-90] All three podial elements appear in the forelimbs at *L. lugubris* stage 32, which matches the timing of most geckos, gymnophthalmids, lacertids, some acrodonts, and anguimorphs, but is earlier than other acrodonts and pleurodonts, and later than other pleurodonts. Finally, fusion of the facial primordia occurs at stage 33 which is the same timing as other geckos, some acrodonts, and anguimorphs, but earlier than lacertids, other acrodonts, and pleurodonts, and later than gymnophthalmids. Along with other squamate taxa, the deviations from these sequences observed in *L. lugubris* in mere three characters, which are considered by some to have gecko-specific character states, suggest widespread heterochrony in squamate development. Further investigations into normal embryonic development of additional taxa are required to determine which developmental characteristics actually are clade-specific.

Squamates are becoming increasingly used as models in evolutionary and developmental neurobiology.[91-93] However, the general difficulty of gross dissection of delicate, soft tissues like the embryonic brain is challenging, especially in small species; this task is facilitated by means of nondestructive imaging methods, such as magnetic resonance imaging (MRI[94]) or diffusible iodine-based contrast-enhanced computed tomography (diceCT[58]). Among amniotes, mammals and avian reptiles exhibit a well-developed telencephalon that possesses derived internal architectures.[93] Alternatively, nonavian reptiles (and squamates in particular) possess relatively smaller telencephalic regions that exhibit the ancestral amniote internal architecture, expanded olfactory regions, and small cerebella.[93,95] Gekkotan brains exhibit average "brain mass:body mass" ratios on par with limbed non-Gekkotan squamates[96] and exhibit further elaboration in size of the main olfactory bulbs.[97] Indeed, the large relative size and cellular structure of gekkotan olfactory bulbs, when compared to other squamate lineages, suggests geckos are olfactory specialists with derived forebrain morphologies.[97-99] Our investigation into the development of *L. lugubris* brain development demonstrates that anterior extension of the forebrain, and the resulting appearance of olfactory bulbs, occurs at approximately stage 33 (Figure 8). Furthermore, the olfactory peduncles, which link the olfactory bulbs with the telencephalon, do not appear to extend much past stage 35, suggesting that elongation and further gross morphological development of the olfactory region occurs postnatally. The cerebellum, which is extremely small in squamates when compared to birds or mammals, does not superficially appear to increase in volume relative to the other regions of the brain. The most substantial change in appearance that occurs is the movement of the pontine flexure, where the cerebellum folds in on itself between stages 30 and 33 (Figure 8). Alternatively, in birds, which have large cerebella that comprise approximately one quarter of the brain,[93] the cerebellum is distinguishable by MRI at 9 dpo (stage 35[45]) and continues to grow rapidly within the next 10 days (stages 35-45[45,68,100]). As nondestructive visualization techniques such as soft-tissue μCT are relatively new, we expect development of resources for additional taxa that will facilitate robust comparative investigations of developmental neuroanatomy.

The annotated transcriptome we presented here provides a description of transcripts expressed in a late-stage *L. lugubris* embryo (i.e., BUSCO score of 83.0%). The presence of most BMPs annotated in the *G. japonicus* genome is evidence of its completeness and utility. Our gene tree, using a subset of recently diverged paralogous BMP genes validated the accuracy of our ortholog assignment. We also corroborate eutherian mammal-specific duplication of BMP8 (i.e., BMP8A and BMP8B[101,102]). Our characterization of the *L. lugubris* embryonic transcriptome will be useful in future investigations of the evolution and development of this species, such as mapping RNAseq reads for differential expression analysis or designing probes for in situ hybridization. Furthermore, the transcriptome may be useful for broader comparative analyses, particularly because there are few genomic resources available for geckos (*G. japonicus*, *E. macularius*, *P. picta*[19,21,24]), and even fewer transcriptomic resources (*E. macularius*, *P. picta*[103,104]).

Robust phylogenetic analysis, genomic information, and detailed developmental data are critical tools to investigate the origins of morphological novelty and convergence. Ideally, by employing a model clade approach, an integrated comparison between closely related taxa with variable phenotypes allows for polarization of ancestral character states and fine-scale investigations into morphological evolution and development.[105] By including another gecko species to the growing number of squamate embryonic staging series, we hope to promote model clade approaches to squamate and vertebrate evo-devo. For example, comparative squamate evo-devo studies that include a gecko and any other non-gekkotan squamate species allow the investigators to sample the phylogenetic breadth of squamates. Furthermore, using geckos themselves as a model clade is becoming more feasible. Currently, normal stages of development are characterized for six gecko species, with varying morphologies and ecologies.[6,53,61,62,72] Access to additional resources — protocols for husbandry and embryo collection,[18,23] genomic

and transcriptomic resources,[19,21,24,103,104] and now manipulatable soft-tissue μCT data across development — sets the foundation for geckos, and specifically *L. lugubris*, to be powerful evo-devo models.

4 | EXPERIMENTAL PROCEDURES

4.1 | Embryo collection and visualization

We collected a post-ovipositional ontogenetic series of 242 embryos from a captive colony of *L. lugubris*, housed at Marquette University (Milwaukee, Wisconsin; IACUC protocol AR-279). The colony includes A and B clonal lineages as well as both diploid and triploid clones[18] and we do not distinguish among them here. Incubation times of *L. lugubris* are known to range between 65 dpo and 103 dpo when incubated at 25.5°C and 22.0°C, respectively.[63] The embryonic series in this study was incubated at approximately 26.0°C (room temperature in the Marquette University live-lizard facility) and spans 0-77 dpo (Figure 1).[106] Captive animals were cared for and embryos were collected following protocols described by Griffing et al.[18] To summarize, we checked animal enclosures daily for eggs. We dissected embryos out of eggs using #5 watchmaker's forceps while immersed in diethyl pyrocarbonate (DEPC) treated, RNase-free 1% phosphate-buffered saline. We visualized the external morphology of embryos under a Nikon SMZ 74ST stereoscope and a Zeiss V16 with Axiocam 305 camera. We visualized three embryos from stages 30, 31, and 32 using whole-mount scanning electron microscopy (SEM) to verify choroid fissure closure, AER formation, and pharyngeal arch fusion (Figure 2). Additionally, we visualized a subset of embryos (N = 13), spanning embryonic stages 30-43, using soft-tissue μCT. To demonstrate the utility of the μCT data for evo-devo research, we describe the prenatal development of the *L. lugubris* brain—a structure that is difficult to visualize three-dimensionally in embryos without careful microdissection. Voucher specimens utilized in this study are housed at Marquette University (Milwaukee, Wisconsin) or the Florida Museum of Natural History (Gainesville, Florida).

4.2 | Computed tomography

We imaged a series of 29 specimens (stages 30–43) using contrast-enhanced microcomputed tomography at the University of Florida's Nanoscale Research Facility. We soaked specimens from stages 30–41 in 0.3% Phosphotungstic acid for 1–3 weeks, and 42–43 in 2.5% aqueous Lugol's Iodine (IKI) for 4 days, following modified protocols from Metscher.[107] Prior to scanning, we embedded specimens in low-melt agar, carefully excised them into in close fitting blocks, placed the blocks into a low-density resealable plastic bag, which we then wrapped around a 2 mm diameter carbon fiber rod and placed in a drill chuck inside the computer numerical controlled stage of a dual tube GE Phoenix V|tome|X M. We scanned the specimens using the 180 kV nanofocus tube, with voltage, current, detector capture time, and rotation angles modified to optimize contrast and signal and minimize artifacts (Table S1). We converted the radiographs to tomograms using Phoenix DatosOS|X reconstruction software and then segmented various regions of interest from the volumes using VGStudioMax 3.3 (VolumeGraphics, Heidelberg, Germany). Tomogram stacks and metadata for all scans are available via www.morphosource.org (see Table S1 for DOIs).

4.3 | Diagnosing developmental stages

We discretized and assigned 16 developmental stages based on external morphology using the embryonic staging series of *E. macularius*,[62] *A. sagrei*,[47] and *Gallus gallus*[45] as guides. We primarily diagnosed stages by qualitative traits with the exception of somite number and mean snout-to-vent length (SVL). We calculated SVL for a sample of 118 embryos using the Fiji v2.0.0 image processing software[108] by measuring from the tip of the craniofacial region, to hindbrain, down through the thorax, and ending immediately posterior of the hindlimb or hindlimb bud. Further investigation into development of different clone lineages may be needed to identify lineage-specific differences in development. However, in this investigation, ontogenetic variation between different clonal lineages of *L. lugubris* appears negligible; therefore, these stage diagnoses may be applied to both A and B clones as well as diploid and triploid lineages, and potentially other *L. lugubris* clone lineages.[34,35]

4.4 | Transcriptome sequencing, assembly, and annotation

To further enable the utility of *L. lugubris* as a developmental model, we sequenced and annotated a transcriptome from a late stage embryo. Transcriptomic resources are vital for investigations in developmental biology as they facilitate use of a wide array of methodologies, including PCR primer design for qPCR; a reference for mapping RNAseq reads; and facilitating the design of probes for in situ hybridization.

We extracted RNA from a whole *L. lugubris* embryo (specimen ID: "BJP18") at 59 dpo (stage 42) and followed a modified protocol for extracting RNA from TRIzol preserved tissue.[109] RNAseq library preparation was identical to methods used by Pinto et al.[110] Briefly, we used the KAPA Stranded mRNA-Seq Kit for Illumina (KR0960 [v5.17]) using oligo-dT beads for mRNA enrichment. We sequenced this RNAseq library on an Illumina HiSeq 2500 at the Medical College of Wisconsin (Milwaukee, Wisconsin; paired-end 125 bp reads).

These reads were submitted to the NCBI Sequence Read Archive (SRA; Bioproject: PRJNA476550; Accession number: SRP150730). We calculated quality statistics and scores from these raw data using FastQC (v0.11.6[111]).

We assembled a de novo transcriptome using the De novo RNA-Seq Assembly Pipeline (DRAP [v1.91][112]), which is a compilation of assembly and quality control scripts using several software packages. Briefly, raw Illumina paired-end reads were trimmed, normalized, and assembled into contigs using Trinity (v2.4.0[113]). DRAP then filters, maps, compacts, and quality assesses the initial Trinity assembly using a series of integrated tools. Overall, DRAP generates an assembled transcriptome with less redundancy, without compromising the completeness, or quality, of the transcriptome assembly.[112] Reference peptide sequences provided for reference mapping in all assemblies and assessment reports were from *G. japonicus* ([21]; GenBank 2 693 898, NCBI RefSeq Assembly v1.1).

We identified candidate open reading frames (coding regions) using TransDecoder (v5.0.2[114]) within the de novo transcripts we assembled. Next, we determined the identity of each transcript by assessing homology between the predicted gene region and annotated proteins from the SwissProt database[115] and Pfam (v31.0[116]) databases using BLASTp (v2.7.1[117]) and Hmmer (v3.1b2[118]), respectively. Finally, we associated these homology searches and gene predictions with each transcript using TransDecoder ([v5.0.2][119]) and appended the final gene predictions to the FASTA headers in the final transcriptome file using SeqKit software package (v0.7.2[120]). We assessed our final transcriptome assembly using two transcriptome benchmarking methods: TransRate (v1.01[70]) and Benchmarking Universal Single-Copy Orthologs (BUSCO, [v3.0][121];) against two different databases (tetrapoda_odb9 and CVG). BUSCO analyses were conducted via the gVolante web server.[122]

To illustrate the utility of this transcriptomic assembly, we used BLAST to identify paralogous sequences in the transcriptome from a subset of a well-studied gene family with important developmental functions, the BMPs (*bmp*).

We downloaded all annotated peptide sequences (BMPs 2, 4-8) from published genomes within the major amniote lineages (mammals: *Homo sapiens* and *Mus musculus*; birds: *G. gallus,* and *Taeniopygia guttata*; crocodilians: *Crocodylus porosus*; turtles: *Pelodiscus sinensis*; and [non-gecko] squamate reptiles: *A. carolinensis* and *Pogona vittatus*) via the Ensembl database [v96]. For geckos, we queried *Anolis* sequences to GenBank to identify the predicted sequence for each BMP gene in *G. japonicus.* We then used these *Gekko* sequences to query the de novo *Lepidodactylus* transcriptome, the *P. picta* genome,[19] and the *E. macularius* genome.[24] To further increase the sampling of squamate reptiles, we also incorporated *Chamaeleo calyptratus* BMP sequences.[110] We aligned each BMP molecule separately using MAFFT [v7.388] implemented in Geneious [v11.1.2].[123,124] Then, used the Geneious consensus alignment function to generate an alignment of all six BMP paralogs. We generated gene trees using the RAxML Blackbox [v8.2.10],[125] under the BLOSUM62 protein substitution matrix, implemented on the CIPRES portal.[126] We rooted the gene tree at the split between the clade containing BMP2 and BMP4 as sister to the clade containing BMPs 5-8, sensu Ducy and Karsenty.[71]

ACKNOWLEDGMENTS

We gratefully acknowledge the hard work of the Institutional Animal Care and Use Committees (IACUC) and employees of the captive animal facilities of Marquette University and Loyola University at Chicago. We also thank the State of Hawaii Division of Forestry and Wildlife for permission to collect *Lepidodactylus lugubris* (Permits: EX09-06, EX12-08) and D. Zarkower and C. Matson for help during field collection. This study was funded in-part by the National Science Foundation (DEB1657662 awarded to TG; DEB1657656 awarded to JDD; DBI1701714 awarded to ELS) and funds from Loyola University Chicago (TJS). Finally, we thank two anonymous reviewers, who contributed comments that benefitted an earlier version of this article.

DATA ACCESSIBILITY

Raw reads for the transcriptome are available on the Sequence Read Archive (NCBI SRA). The assembled, annotated transcriptome and BMP alignment and tree (in nexus format) are available on Figshare (DOI: 10.6084/m9.figshare.7823690). μCT image stack data is available on MorphoSource (project 543; DOIs available in Supplementary Table).

ORCID

Aaron H. Griffing https://orcid.org/0000-0001-8441-1330
Thomas J. Sanger https://orcid.org/0000-0003-0047-1884
Juan D. Daza https://orcid.org/0000-0002-5651-0240
Stuart V. Nielsen https://orcid.org/0000-0002-3114-1469
Brendan J. Pinto https://orcid.org/0000-0002-4243-5788
Edward L. Stanley https://orcid.org/0000-0001-5257-037X
Tony Gamble https://orcid.org/0000-0002-0204-8003

REFERENCES

1. Cohn MJ, Tickle C. Developmental basis of limblessness and axial patterning in snakes. *Nature*. 1999;399:474-479.
2. Diaz RE Jr, Bertocchini F, Trainor PA. Lifting the veil on reptile embryology: the veiled chameleon (*Chamaeleo calyptratus*) as a

model system to study reptilian development. In: Sheng G, ed. *Avian and Reptilian Developmental Biology*. New York: Humana Press; 2017:269-284.
3. Infante CR, Rasys AM, Menke DB. Appendages and gene regulatory networks: lessons from the limbless. *Genesis*. 2018;56:e23078.
4. Leal F, Cohn MJ. Developmental, genetic, and genomic insights into the evolutionary loss of limbs in snakes. *Genesis*. 2018;56: e23077.
5. Nomura T, Yamashita W, Gotoh H, Ono K. Genetic manipulation of reptilian embryos: toward an understanding of cortical development and evolution. *Front Neurosci*. 2015;9:1-11.
6. Noro M, Uejima A, Abe G, Manabe M, Tamura K. Normal developmental stages of the Madagascar ground gecko *Paroedura pictus* with special reference to limb morphogenesis. *Dev Dyn*. 2009;238:100-109.
7. Sanger TJ, Kircher BK. Model clades versus model species: *Anolis* lizards as an integrative model of anatomical evolution. In: Sheng G, ed. *Avian and Reptilian Developmental Biology*. New York: Humana Press; 2017:285-297.
8. Jenner RA, Wills MA. The choice of model organisms in evo–deva. *Nat Rev Genet*. 2007;8:311-314.
9. Conrad JL. Phylogeny and systematics of Squamata (Reptilia) based on morphology. *Bull Am Museum Nat Hist*. 2008;310: 1-182.
10. Gamble T, Greenbaum E, Jackman TR, Russell AP, Bauer AM. Repeated origin and loss of adhesive toepads in geckos. *PLoS One*. 2012;7:e39429.
11. Russell AP, Baskerville J, Gamble T, Higham TE. The evolution of digit form in *Gonatodes* (Gekkota: Sphaerodactylidae) and its bearing on the transition from frictional to adhesive contact in gekkotans. *J Morphol*. 2015;276:1311-1332.
12. Russell AP, Gamble T. Evolution of the gekkotan adhesive system: does digit anatomy point to one or more origin? *Integr Comp Biol*. 2019. https://doi.org/10.1093/icb/icz006.
13. Russell AP. Parallelism and integrated design in the foot structure of gekkonine and diplodactyline geckos. *Copeia*. 1979;1979: 1-21.
14. Gamble T, Coryell J, Ezaz T, Lynch J, Scantlebury DP, Zarkower D. Restriction site-associated DNA sequencing (RAD-seq) reveals an extraordinary number of transitions among Gecko sex-determining systems. *Mol Biol Evol*. 2015a;32:1296-1309.
15. Gamble T, Greenbaum E, Jackman TR, Bauer AM. Into the light: diurnality has evolved multiple times in geckos. *Biol J Linn Soc*. 2015b;115:896-910.
16. Reeder TW, Townsend TM, Mulcahy DG, et al. Integrated analyses resolve conflicts over squamate reptile phylogeny and reveal unexpected placements for fossil taxa. *PLoS One*. 2015; 10:e0118199.
17. Zheng Y, Wiens JJ. Combining phylogenomic and supermatrix approaches, and a time-calibrated phylogeny for squamate reptiles (lizards and snakes) based on 52 genes and 4162 species. *Mol Phylogenet Evol*. 2016;94:537-547.
18. Griffing AH, Sanger TJ, Matamoros IC, Nielsen SV, Gamble T. Protocols for husbandry and embryo collection of a parthenogenetic gecko, *Lepidodactylus lugubris* (Squamata: Gekkonidae). *Herpetol Rev*. 2018;49:230-235.
19. Hara Y, Takeuchi M, Kageyama Y, et al. Madagascar ground gecko genome analysis characterizes asymmetric fates of duplicated genes. *BMC Biol*. 2018;16:40.
20. Koepfli K-P, Paten B, Antunes A, et al. The genome 10K project: a way forward. *Annu Rev Anim Biosci*. 2015;3:57-111.
21. Liu Y, Zhou Q, Wang Y, et al. *Gekko japonicus* genome reveals evolution of adhesive toe pads and tail regeneration. *Nat Commun*. 2015;6:10033.
22. Thorogood J, Whimster IW. The maintenance and breeding of the leopard gecko, *Eublepharis macularius*, as a laboratory animal. *Int Zoo Yearb*. 1979;19:74-78.
23. Vickaryous MK, Gilbert EAB. Reptile embryology and regeneration. In: Pelegri FJ, ed. *Vertebrate Embryogenesis*. New York: Humana Press; 2019:219-246.
24. Xiong Z, Li F, Li Q, et al. Draft genome of the leopard gecko, *Eublepharis macularius*. *Gigascience*. 2016;5:47.
25. Uetz P, Freed P, Hošek J. 2018. The Reptile Database. www.reptile-database.org.
26. Bauer AM, Henle KH. *Das Tierreich Part 109: Familia Gekkonidae (Reptilia, Sauria). Part I: Australia and Oceania*. Berlin: Walter de Gruyter; 1994:324.
27. Röll B. *Lepidodactylus lugubris* (Duméril & Bibron). *Sauria*. 2002;24:545-550.
28. Brown RM, Siler CD, Das I, Min Y. Testing the phylogenetic affinities of Southeast Asia's rarest geckos: flap-legged geckos (*Luperosaurus*), flying geckos (*Ptychozoon*) and their relationship to the pan-Asian genus *Gekko*. *Mol Phylogenet Evol*. 2012; 63:915-921.
29. Kluge AG. Phylogenetic relationships of the gekkonid lizard genera *Lepidodactylus* Fitzinger, *Hemiphyllodactylus* Bleeker, and *Pseudogekko* Taylor. *Philipp J Sci*. 1968;95:331-352.
30. Bustard HR. The egg-shell of gekkonid lizards: a taxonomic adjunct. *Copeia*. 1968;1968:162-164.
31. Cuellar O, Kluge AG. Natural parthenogenesis in the gekkonid lizard *Lepidodactylus lugubris*. *J Genet*. 1972;61:14-26.
32. Brown SG, Murphy-Walker S. Behavioral interactions between a rare male phenotype and female unisexual *Lepidodactylus lugubris*. *Herpetol J*. 1996;6:69-73.
33. Röll B, von Düring MUG. Sexual characteristics and spermatogenesis in males of the parthenogenetic gecko *Lepidodactylus lugubris* (Reptilia, Gekkonidae). *Fortschr Zool*. 2008;111: 385-400.
34. Radtkey RR, Donnellan SC, Fisher RN, Moritz C, Hanley KA, Case TJ. When species collide: the origin and spread of an asexual species of gecko. *Proc R Soc B*. 1995;259:145-152.
35. Moritz C, Case TJ, Bolger DT, Donnellan S. Genetic diversity and the history of pacific Island house geckos (*Hemidactylus* and *Lepidodactylus*). *Biol J Linn Soc*. 1993;48:113-133.
36. Maynard-Smith J. What use is sex? *J Theor Biol*. 1971;30: 319-335.
37. Cole CJ, Townsend CR. Parthenogenetic reptiles: new subjects for laboratory study. *Experientia*. 1977;33:285-410.
38. Darevsky IS, Kupriyanova LA, Uzzell T. Parthenogenesis in reptiles. In: Gans C, Billett F, eds. *Biology of the Reptilia, Volume 15, Development B*. New York: John Wiley & Sons; 1985: 411-526.
39. Kearney M, Shine R. Developmental success, stability, and plasticity in closely related parthenogenetic and sexual lizards (*Heteronotia*, Gekkonidae). *Evolution*. 2004;58:1560-1572.
40. Lutes AA, Neaves WB, Baumann DP, Wiegräbe W, Baumann P. Sister chromosome pairings maintains heterozygosity in parthenogenetic lizards. *Nature*. 2010;464:283-286.

41. Maslin TP. Conclusive evidence of parthenogenesis in three species of *Cnemidophorus* (Teiidae). *Copeia*. 1971;1971:156-158.
42. Townsend CR. Establishment and maintenance of colonies of parthenogenetic whiptail lizards: *Cnemidophorus spp*. *Int Zoo Yearb*. 1979;19:80-86.
43. Brown SG, Sakai TJY. Social experience and egg development in the parthenogenic gecko, *Lepidodactylus lugubris*. *Ethology*. 1998;79:317-325.
44. Greenbaum E. A standardized series of embryonic stages for the emydid turtle *Trachemys scripta*. *Can J Zool*. 2002;80:1350-1370.
45. Hamburger V, Hamilton HL. A series of normal stages in the development of the chick embryo. *J Morphol*. 1951;88:49-92.
46. Hopwood N. A history of normal plates, tables and stages in vertebrate embryology. *Int J Dev Biol*. 2007;51:1-26.
47. Sanger TJ, Losos JB, Gibson-Brown JJ. A developmental staging series for the lizard genus *Anolis*: a new system for the integration of evolution, development, and ecology. *J Morphol*. 2008; 269:129-137.
48. Schreckenberg GM, Jacobson AG. Normal stages of development of the Axolotl, *Ambystoma mexicanum*. *Dev Biol*. 1975;42:391-400.
49. Peter K. Normentafeln zur entwicklungsgeschichte der zauneidechse (*Lacerta agilis*). In: Keibel F, ed. *Normentafeln Zur Entwicklungsgeschichte Der Wirbeltiere*. Jena: Gustav Fischer; 1904:1-165.
50. Lima FC, Py-Daniel TR, Sartori MR, et al. Developmental staging table of the green iguana. *Acta Zool*. 2019;100:232-244.
51. Iungman JL, Molinero MN, Simoncini MS, Piña CI. Embryological development of *Salvator merianae* (Squamata: Teiidae). *Genesis*. 2019;57:e23280.
52. Ollonen J, Da Silva FO, Mahlow K, Di-Poï N. Skull development, ossification pattern, and adult shape in the emerging lizard model organism *Pogona vitticeps*: a comparative analysis with other squamates. *Front Physiol*. 2018;9:1-26.
53. Vos WVD, Stein K, Di-poï N, Bickelmann C, Penner J. Ontogeny of *Hemidactylus* (Gekkota, Squamata) with emphasis on the limbs. *Zoosystem Evol*. 2018;94:195-209.
54. Hogan BLM. Bone morphogenetic proteins: multifunctional regulators of vertebrate development. *Genes Dev*. 1996;10:1580-1594.
55. Polachowski KM, Werneburg I. Late embryos and bony skull development in *Bothropoides jararaca* (Serpentes, Viperidae). *Fortschr Zool*. 2013;116:36-63.
56. Werneburg I, Polachowski KM, Hutchinson MN. Bony skull development in the Argus monitor (Squamata, Varanidae, *Varanus panoptes*) with comments on developmental timing and adult anatomy. *Fortschr Zool*. 2015;118:255-280.
57. Boughner JC, Buchtová M, Fu K, Diewert V, Hallgrímsson B, Richamn JM. Embryonic development of *Python sebae* – I: staging criteria and macroscopic morphogenesis of the head and limbs. *Fortschr Zool*. 2007;11:212-230.
58. Gignac PM, Kley NJ, Clarke JA, et al. Diffusible iodine-based contrast-enhanced computed tomography (diceCT): an emerging tool for rapid, high-resolution, 3-D imaging of metazoan soft tissues. *J Anat*. 2016;228:889-909.
59. Wong MD, Dorr AE, Walls JR, Lerch JP, Henkelman RM. A novel 3D mouse embryo atlas based on micro-CT. *Development*. 2012;139:3248-3256.
60. Dufaure JP, Hubert J. Table de développment du lézard vivipare: *Lacerta* (*Zootoca*) *vivipara* Jacquin. *Arch Anat Microsc Morphol Exp*. 1961;50:309-327.
61. Khannoon ER. Developmental stages of the climbing gecko *Tarentola annularis* with special reference to the claws, pad lamellae, and subdigital setae. *J Exp Zool Part B Mol Dev Evol*. 2015; 324:450-464.
62. Wise PAD, Vickaryous MK, Russell AP. An embryonic staging table for in ovo development of *Eublepharis macularius*, the leopard gecko. *Anat Rec*. 2009;292:1198-1212.
63. Brown SG, Murphy-Walker S. The effects of egg-laying site, temperature, and salt water on incubation time and hatching success in the gecko *Lepidodactylus lugubris*. *J Herpetol*. 1992;26: 510-513.
64. Gredler ML, Sanger TJ, Cohn MJ. Development of the cloaca, hemipenes, and hemiclitores in the green anole, *Anolis carolinensis*. *Sex Dev*. 2015;9:21-33.
65. Whiteley SL, Weisbecker V, Georges A, Gauthier ARG, Whitehead DL, Holleley CE. Developmental asynchrony and antagonism of sex determination pathways in a lizard with temperature-induced sex reversal. *Sci Rep*. 2018;8:14892.
66. Roth LSV, Lundström L, Kelber A, Kröger RHH, Unsbo P. The pupils and optical systems of gecko eyes. *J Vis*. 2009;9:27-2711.
67. Arey LB. *Developmental Anatomy*. 7th ed. Philadelphia: W. B. Saunders Company; 1974:695.
68. Bellairs R, Osmond M. *The Atlas of Chick Development*. 2nd ed. Elsevier Academic Press: San Diego; 2005:470.
69. Senn DG. Embryonic development of the central nervous system. In: Gans C, Northcutt RG, Ulinski P, eds. *Biology of the Reptilia, Volume 9, Neurology A*. London: Academic Press; 1979: 173-244.
70. Smith-Unna R, Boursnell C, Patro R, Hibberd JM, Kelly S. TransRate: reference-free quality assessment of de novo transcriptome assemblies. *Genome Res*. 2016;26:1134-1144.
71. Ducy P, Karsenty G. The family of bone morphogenetic proteins. *Kidney Int*. 2000;57:2207-2214.
72. Zhao R-N, Zhang L-Y, Wu P-F, Ping J, Jin J-Y, Zhang Y-P. The morphological characteristics of embryos at different developmental stages in the Japanese gecko, *Gekko japonicus*. *Chin J Zool*. 2017;52:987-995.
73. Andrews RM. Patterns of embryonic development. In: Deeming D, ed. *Reptilian Incubation: Environment, Evolution and Behavior*. Nottingham: Nottingham University Press; 2004: 75-102.
74. Andrews RM, Thompson MB, Greene VW. Does low gas permeability of rigid-shelled gekkotan eggs affect embryonic development? *J Exp Zool*. 2013a;319A:259-267.
75. Pike DA, Andrews RM, Du W. Eggshell morphology and gekkotan life-history evolution. *Evol Ecol*. 2012;26:847-861.
76. Rieppel O. Studies on skeleton formation in reptiles. Patterns of ossification in the limb skeleton of *Gehyra oceanica* (lesson) and *Lepidodactylus lugubris* (Duméril & Bibron). *Ann Sci Nat Zool Biol Anim*. 1994;15:83-91.
77. Rieppel O. The structure of the skull and jaw adductor musculature in the Gekkota, with comments on the phylogenetic relationship of the Xantusiidae (Reptilia: Lacertilia). *Zool J Linn Soc*. 1984;82:291-318.
78. Andrews RM. Water vapor permeability of the rigid-shelled Gecko egg. *J Exp Zool*. 2012;317A:395-400.
79. Kluge AG. Higher taxonomic categories of gekkonid lizards and their evolution. *Bull Am Nat Mus Hist*. 1967;135:1-60.

80. Rösler H. Die Eizähne einiger Geckos (Reptilia: Gekkota). *Gekkota*. 2001;3:99-124.
81. Gredler ML, Larkins CE, Leal F, et al. Evolution of external genitalia: insights from reptilian development. *Sex Dev*. 2014;8:311-326.
82. Raynaud A, Pieau C. Embryonic development of the genital system. In: Gans C, Billett F, eds. *Biology of the Reptilia, Volume 15, Development B*. New York: John Wiley & Sons; 1985: 149-300.
83. Martínez-Torres M, Rubio-Morales B, Piña-Amado JJ, Luis J. Hemipenes in females of the Mexican viviparous lizard *Barisia imbricata* (Squamata: Anguidae): an example of heterochrony in sexual development. *Evol Dev*. 2015;17:270-277.
84. Andrews RM, Brandley MC, Greene VW. Developmental sequences of squamate reptiles are taxon specific. *Evol Dev*. 2013b;15:326-343.
85. Py-Daniel TR, De-Lima AKS, Lima FC, Pic-Taylor A, Pires OR Jr, Sebben A. A staging table of post-ovipositional development for the South American collared lizard *Tropidurus torquatus* (Squamata: Tropiduridae). *Anat Rec*. 2017;300:277-290.
86. Hubert J. Embryology of the squamata. In: Gans C, Billett F, eds. *Biology of the Reptilia, Volume 15, Development B*. New York: John Wiley & Sons; 1985:1-34.
87. Gregorovicova M, Zahradnicek O, Tucker AS, Velensky P, Horacek I. Embryonic development of the monitor lizard, *Varanus indicus*. *Amphib Reptil*. 2012;33:451-468.
88. Muthukkaruppan VR, Kanakambika P, Manickavel V, Veeraraghavan K. Analysis of the development of the lizard, *Calotes versicolor*. *J Morphol*. 1970;130:479-490.
89. Roscito JG, Rodrigues MR. Embryonic development of the fossorial gymnophthalmid lizards *Nothobachia ablephara* and *Calyptommatus sinebrachiatus*. *Fortschr Zool*. 2012;115:302-318.
90. Whiteley SL, Holleley CE, Ruscoe WA, et al. Sex determination mode does not affect body or genital development of the central bearded dragon (*Pogona vitticeps*). *Evodevo*. 2017;8:25.
91. Desfilis E, Abellán A, Sentandreu V, Medina L. Expression of regulatory genes in the embryonic brain of a lizard and implications for understanding pallial organization and evolution. *J Comp Neurol*. 2018;526:166-202.
92. Hoops D. The secret caverns of the dragon's brain: current and potential contributions of lizards to evolutionary neuroscience. *Brain Behav Evol*. 2018;91:1-3.
93. Nomura T, Kawaguchi M, Ono K, Murakami Y. Reptiles: a new model for brain evo-devo research. *J Exp Zool (Mol Dev Evol)*. 2013;9999B:1-17.
94. Hoops D, Desfilis E, Ullmann JFP, et al. A 3D MRI-based atlas of a lizard brain. *J Comp Neurol*. 2018;526:2511-2547.
95. Bruce LL. Evolution of the nervous system in reptiles. In: Kaas JH, ed. *Evolution of Nervous Systems*. Waltham: Academic Press; 2007:125-156.
96. De Meester G, Huyghe K, Van Damme R. Brain size, ecology and sociality: a reptilian perspective. *Biol J Linn Soc*. 2019;126:381-391.
97. Smeets WJAJ, Hoogland PV, Lohman AHM. A forebrain atlas of the lizard *Gekko gecko*. *J Comp Neurol*. 1986;254:1-19.
98. Rehorek SJ, Firth BT, Hutchinson MN. The structure of the nasal chemosensory system in squamate reptiles. 1. The olfactory organ, with special references to olfaction in geckos. *J Biosci*. 2000;25:173-179.
99. Schwenk K. Are geckos olfactory specialists? *J Zool Lond*. 1993; 229:289-302.
100. Zhou Z, Chen Z, Shan J, et al. Monitoring brain development of chick embryos in vivo using 3.0 T MRI: subdivision volume change and preliminary structural quantification using DTI. *BMC Dev Biol*. 2015;15:29.
101. Carson AR, Scherer SW. Identifying concerted evolution and gene conversion in mammalian gene pairs lasting over 100 million years. *BMC Evol Biol*. 2009;9:156.
102. Zhao G-Q, Hogan BLM. Evidence that mouse *Bmp8a* (*Op2*) and *Bmp8b* are duplicated genes that play a role in spermatogenesis and placental development. *Mech Dev*. 1996;57:159-168.
103. Hara Y, Tatsumi K, Yoshida M, Kajikawa E, Kiyonari H, Kuraku S. Optimizing and benchmarking *de novo* transcriptome sequencing: from library preparation to assembly evaluation. *BMC Genomics*. 2015;16:977.
104. Tzika AC, Ullate-Agote A, Grbic D, Milinkovitch MC. Reptilian transcriptomes v2.0: an extensive resource for Sauropsida genomics and transcriptomics. *Genome Biol Evol*. 2015;7:1827-1841.
105. Sanger TJ, Rajakumar R. How a growing organismal perspective is adding new depth to integrative studies of morphological evolution. *Biol Rev*. 2019;94:184-198.
106. R Core Team. *R: A Language and Evironment for Statistical Computing*. Vienna, Austria: R Foundation for Statistical Computing; 2014.
107. Metscher B. Micro-CT for comparative morphology: simple staining methods allow high-contrast 3D imaging of diverse non-mineralized animal tissues. *BMC Physiol*. 2009;9:1-11.
108. Schindelin J, Arganda-Carreras I, Frise E, et al. Fiji: an open-source platform for biological-image analysis. *Nat Methods*. 2012;9:676-682.
109. Zumbo P. 2011. Isolate ($\leq$ 45 ug) Total RNA from (5×10^5) Animal Cells. http://physiology.med.cornell.edu/faculty/mason/lab/zumbo/files/ZUMBO_rna_isolation_cells.pdf
110. Pinto BJ, Card DC, Castoe TA, et al. The transcriptome of the veiled chameleon (*Chamaeleo calyptratus*): a resource for studying the evolution and development of vertebrates. *Dev Dyn*. 2019. https://doi.org/10.1002/dvdy.20
111. Andrews S. 2010. FastQC: a Quality Control Tool for High Throughput Sequence Data. http://www.bioinformatics.babraham.ac.uk/projects/fastqc
112. Cabau C, Escudié F, Djari A, Guiguen Y, Bobe J, Klopp C. Compacting and correcting trinity and oases RNA-seq de novo assemblies. *PeerJ*. 2017;5:e2988.
113. Grabherr MG, Haas BJ, Yassour M, et al. Trinity: reconstructing a full-length transcriptome without a genome from RNA-Seq data. *Nat Biotechnol*. 2011;29:644-652.
114. Haas B. 2015. TransDecoder (Find Coding Regions Within Transcripts). https://github.com/TransDecoder
115. The UniProt Consortium. UniProt: the universal protein knowledgebase. *Nucleic Acids Res*. 2017;45:D158-D169.
116. Finn RD, Coggill P, Eberhardt RY, et al. The Pfam protein families database: towards a more sustainable future. *Nucleic Acids Res*. 2016;44:D279-D285.
117. Altschul SF, Gish W, Miller W, Myers EW, Lipman DJ. Basic local alignment search tool. *J Mol Biol*. 1990;215:403-410.
118. Finn RD, Clements J, Eddy SR. HMMER web server: interactive sequence similarity searching. *Nucleic Acids Res*. 2011;39:W29-W37.
119. Haas BJ, Papanicolaou A, Yassour M, et al. De novo transcript sequence reconstruction from RNA-seq using the Trinity platform for reference generation and analysis. *Nat Protoc*. 2013;8: 1494-1512.

120. Shen W, Le S, Li Y, Hu F. SeqKit: a cross-platform and ultrafast toolkit for FASTA/Q file manipulation. *PLoS One*. 2016;11: e0163962.
121. Simão FA, Waterhouse RM, Ioannidis P, Kriventseva EV, Zdobnov EM. BUSCO: assessing genome assembly and annotation completeness with single-copy orthologs. *Bioinformatics*. 2015;31:3210-3212.
122. Nishimura O, Hara Y, Kuraku S. gVolante for standardizing completeness assessment of genome and transcriptome assemblies. *Bioinformatics*. 2017;33:3635-3637.
123. Katoh K, Misawa K, Kuma K-I, Miyata T. MAFFT: a novel method for rapid multiple sequence alignment based on fast Fourier transform. *Nucl Acids Res*. 2002;30:3059-3066.
124. Kearse M, Moir R, Wilson A, et al. Geneious Basic: an integrated and extendable desktop software platform for the organization and analysis of sequence data. *Bioinformatics*. 2012;28:1647-1649.
125. Stamatakis A. RAxML version 8: a tool for phylogenetic analysis and post-analysis of large phylogenies. *Bioinformatics*. 2014;30:1312-1313.
126. Miller MA, Pfeiffer W, Schwartz T. *Creating the CIPRES Science Gateway for inference of large phylogenetic trees*. Proceedings of the 2010 Gateway Computing Environments Workshop (GCE 2010); November 14, 2010, New Orleans, LA, pp 1–8.

SUPPORTING INFORMATION

Additional supporting information may be found online in the Supporting Information section at the end of this article.

How to cite this article: Griffing AH, Sanger TJ, Daza JD, et al. Embryonic development of a parthenogenetic vertebrate, the mourning gecko (*Lepidodactylus lugubris*). *Developmental Dynamics*. 2019;248:1070–1090. https://doi.org/10.1002/dvdy.72